Journal of Applied Fluid Mechanics, Vol. 17, No. 1, pp. 19-42, 2024.
Available online at www.jafmonline.net, ISSN 1735-3572, EISSN 1735-3645.
https://doi.org/10.47176/jafm.17.1.1927

A Methodology for Designing a Fish-Friendly Turbine Rotor Applied to High-Power Generation

G. E. Niño Del Río†, R. G. Ramirez Camacho, N. Manzanares Filho, W. de Oliveira and T. M. Arispe Angulo

Federal University of Itajubá, Itajubá, Minas Gerais, Zip Code 37500 903, Brazil

†*Corresponding Author Email: ge.nino@unifei.edu.br*

ABSTRACT

Most large hydropower facilities employing conventional hydraulic turbines, e.g., Francis, Kaplan, or Bulb turbines, etc., cause significant harm to fish, resulting in high mortality rates, during turbine operation. This results from strong injury-inducing mechanisms at the rotor, including shear stresses, pressure variations, and pressure drop through the rotor. The study outlines a methodology for designing a fish-friendly turbine that is suitable for high-power generation applications. This methodology for a hydraulic channel design within the turbine rotor was derived based on classical fundamental applications of a rotor design, supplemented by subsequent assessments that incorporate fish-friendly design parameters that have been documented in the existing literature. A spiral curve characterized by a linear angle variation between the rotor's inlet and outlet was employed to project the blade geometry. Here, the Göttingen hydrofoil series was used, while a second-order polynomial function guided the hub design. Both of these parametrizations sought to enhance the turbine's hydraulic efficiency. Minimum Absolute Pressure, Strain Rate, and Pressure Variation Rate intervals were established as assessment criteria for fish survival for certain species, as has also been previously explored in the literature. The findings were outlined in terms of hydrodynamic performance and flow behavior within the rotor. An improvement in hydraulic efficiency was observed, transitioning from a Preliminary Turbine geometry design to an Optimized Turbine Geometry design. The turbine rotor was optimized using Computational Fluid Dynamics (CFD) simulations, generated from a Design of Experiments (DOE). Modifications to the hydrofoil type, the sweep angle, and the trailing edge angle of the blades were all made, coupled with integrations of assessments considering fish-friendly parameters.

Article History

Received April 16, 2023
Revised August 23, 2023
Accepted August 29, 2023
Available online November 1, 2023

Keywords:

Fish-Friendly Turbine Rotor
Spiral curve
Linear angle variation
Hydraulic performance
Design
Optimization
CFD

1. INTRODUCTION

Historically and contemporarily, the primary objective of hydraulic turbine designs has been to create high-efficiency rotors, while accounting for variables like volumetric flow, height, and rotation. Today, environmental protection regulations are an integral part of the design process, helping reduce fish mortality rates as fish pass through the turbines. Currently, many hydraulic turbines, operating across a wide range of heads (high, medium, and low) and in different configurations e.g., Francis, Kaplan, or Bulb turbines, result in injuries to fish, as has been shown by Amaral et al. (2011) and Mueller et al. (2017). One cause of fish mortality, according to Loures (2012), is when turbines start up, leading quickly to pronounced variations in pressure and speed. However, more gradual start-ups may result in damage to the guide bearing and thrust bearing.

Various injury mechanisms that are present in the passageway through the turbine elevate fish mortality rates, thereby significantly decreasing fish survival rates. These injury factors affecting fish as they traverse the hydraulic channel of the turbine are primarily associated with high-pressure gradients, cavitation, shear forces, impacts against mechanical components (e.g., blade strikes), and grinding. These phenomena occur in the spaces between the fixed and moving parts of the turbine, as detailed by Odeh (1999) and Čada (2001).

NOMENCLATURE

BEP	Best Efficiency Point	r_{int}	Radius at the intersection point between the straight lines of the hub construction
BD	Base Design	t	Blade pitch (Dimensionless)
b	Blade width	u	Tangential velocity
c	Absolute velocity	w	Relative velocity
cm	Meridional component velocity	w_u	Relative velocity projected at the u direction
cu	Absolute velocity component in the u direction	Y	Specific energy
e	Blade thickness	$Y_{pá\infty}$	Specific energy - infinite blade number
es	Superior thickness of the hydrodynamic profile	y^+	y^+ value (Dimensionless)
et	Blade thickness measured in the tangential direction	zi_{nt}	Height at the intersection point between the straight lines of the hub construction
DH	Hydraulic diameter	α	Absolute flow velocity angle
D	Rotor diameter	β	Relative flow velocity angle
D_{pmean}	Distance of the mean point of the second-order polynomial curve	Δz_n	Height of the mean curvature among the last discretized points at the mid-blade
fe	Obstruction factor (dimensionless)	δ	Hub construction angle at the rotor inlet
H	Liquid height	ε	Turbulent dissipation rate; Strain rate
k	Turbulent kinetic energy	$\in$	Residuals Mean Square (RMS)
h	Hub height	ζ	Loss coefficient of the draft tube
L_{mp}	Length of the mean curvature at the mid-blade	γ	Hub construction angle of the rotor outlet
L_n	Length of the mean curvature at the mid-blade between the last discretized points	λ	Opening blade angle
n	Angular velocity in [rpm] or [rps]	ξ	Complementary angle of the γ angle
N_{blade}	Blade number (Dimensionless)	η_h	Hydraulic efficiency (Dimensionless)
n_{qA}	Addison number for specific rotation (Dimensionless)	η_l	Leakage efficiency
PD	Preliminary Design	η_{lf}	Lateral friction efficiency
Pt	Total pressure	η_m	Mechanical efficiency
P_{abmin}	Minimum absolute pressure	θ	Blade sweep angle
p_7	Static pressure	ρ	Specific mass
OG	Optimized Geometry	φ	Complementary angle at the G edge of the triangle EFG
Q	Volumetric flow of the rotor	ω	Angular velocity; Specific Energy Dissipation rate
r	Radius through the passageway at the hub root		

The importance of designing a fish-friendly turbine lies in achieving high hydraulic performance and efficiency without compromising fish species. This approach plays a vital role in minimizing the impacts of various fish injury mechanisms encountered when fish pass through the turbine, as previously described.

The advantages offered by this type of turbine, specifically in terms of fish survival rates compared to other conventional turbine types, include the following:

- A reduction in the number of blades, relative to other turbine types like the Francis or Bulb turbines, thus decreasing the probability that fish will hit the rotor blades. The likelihood of striking the blade grows significantly with an increase in the number of blades on the rotor. (Larinier & Dartiguelongue 1989; Hecker et al., 2012, among others)
- A shroud fixed with the turbine rotor, rotating in unison with the rotor, avoids the fish grinding, which is a known mechanism for causing fish mortality. This issue is common to conventional hydraulic turbines like the Kaplan, Francis, and Bulb turbines, where the mobile components of the rotor (blades) have clearances greater than 2 mm with the fixed components. Dixon and Dham (2011).
- This turbine type does not interrupt the reproductive cycles of various fish species, e.g., salmon. These fish need to travel upstream in rivers to lay their eggs for reproduction. Odeh (1999).
- One design consideration for this type of turbine is maintaining a lower pressure drop, in terms of Nadir pressure, at the absolute pressure immediately after the flow passes through the rotor, ensuring that it remains within a permissible range that would allow for fish survival. (See Odeh, 1999), and U.S. Environmental Protection Agency criteria, cited by Cooke et al., 2011).
- The hydraulic channel between the rotor's blades must be wide enough along its length to avoid high strain rates in the inner flow, due to elevated shear

stresses on the rotor walls. (Odeh, 1999; Dixon & Dham, 2011).

Many researchers have conducted wide and extensive investigations into the development of fish-friendly turbines, as well as on various fish injury mechanisms.

Deng et al. (2005) conducted an evaluation of fish-injury mechanisms related to exposure to turbulent shear flows in juvenile salmon. The fish were introduced into a flume and exposed to a submerged water jet to quantify shear stress injuries and fish mortality rates, simulating an environment similar to a hydraulic turbine. Furthermore, Ploskey and Carlson (2004) compared blade-strike modeling results with empirical data.

Hecker et al. (2012) presented a strike blade fish mortality probability model equation for the Alden Turbine type, showing that a rotor with more blades strongly increases the probability of blade strikes to fish, which is one of the main causes of fish mortality.

Regarding pressure gradients and pressure variation rates, Barotrauma causes physiological damage, like ruptures to the swimming bladder, exophthalmia, internal hemorrhaging, and emboli, due to gas bubble formation, leading to fish mortality, as mentioned in Abernethy et al. (2003) and Brown et al. (2012, 2014).

In Richmond et al. (2014), a method for assessing hydro turbine biological performance was developed and applied to estimate barotrauma-induced mortal injury rates for Chinook salmon exposed to rapid pressure changes in Kaplan-type hydro turbines, using Computational Fluid Dynamics (CFD) techniques.

Similarly, hydropower facilities have conducted experimental and numerical studies using various techniques to quantify the pressure variations and strain rates to which fish are exposed during different stages of hydropower generation. Trumbo et al. (2014) provided a detailed overview of pressure and barotrauma data collection on fish passages through large Kaplan turbines, and these analyses sought to better understand pressure effects on juvenile Chinook salmon and the factors that influence barotrauma, by simulating passage through a turbine.

In a study by Langford et al. (2015), measurements and numerical simulations were conducted to ascertain the velocity and pressure fields upstream of the dam within a hydropower generation facility.

Similarly, in Fu et al. (2016), an *in situ* evaluation was made using an autonomous sensor device to collect data related to the hydraulic conditions that fish experience when passing through Francis turbines (at the Arrowrock, Cougar, and Detroit Dams). The hydraulic conditions measured by the sensors included the Nadir Pressure, pressure gradients, pressure variation rates in the runner region, and collisions and shear stresses in each region of the turbine passageway.

Injury mechanisms like shear stress, as reported by Deng et al. (2005), blade strikes, as per Hecker et al. (2012), along with factors associated with barotrauma effects, per Fu et al. (2016), and grinding, per Brown et al. (2012), may all lead to immediate or delayed fish mortality.

The primary objective of current hydraulic turbine designs has been to achieve high efficiency in hydropower generation. However, there are additional environmental concerns related to the impacts of hydraulic turbine designs on natural resources, including on fish survival rates, and conditions conducive to their natural life cycles. Thus, additional project variables have been introduced to create adapted rotor channels that promote fish survival, and in these designs, modifications are made to fixed components, gaps, and sharp edges on hydrodynamic components to prevent the fish from being hit or injured, as cited in Dixon and Dham (2011) and the U.S. Corps of Army Engineers (2016), among others.

Environmental policies in various nations have started a global trend towards pursuing sustainable development that preserves natural resources and fauna. The United States of America is one of the leading countries in these efforts. The U.S. Department of Energy, in collaboration with key private industry stakeholders, have made enhancements to existing hydraulic turbines, as cited by Odeh (1999) and Čada (2001). Concurrently, a new helical fish-friendly turbine has been developed, resulting from several years of research (Odeh, 1999; Cook et al., 2000; Hecker & Cook, 2005; Dixon & Dham, 2011; Hecker et al., 2012).

Dixon and Dham (2011), and ALDEN and VOITH, building on prior research, tested an enhanced fish-friendly turbine using Computational Fluid Dynamics (CFD) techniques and small-scale model experimental testing. Alden and Voith conducted a case study as a basis for a potential pilot program at Brookfield Renewable's School Street Power Station in upstate New York. Similarly, Nielsen et al. (2015) conducted a review on a case study for installing ALDEN VOITH turbines in the bays of a powerhouse located on the Columbia River in the USA. Nielsen et al. (2015) also studied Alden Voith turbines in another review on the effectiveness and economics of fish-friendly turbines in the Mekong River in Asia.

Nuernbergk and Rorres (2013) formulated an analytical model for water inflows in an Archimedes screw used for hydropower generation. Given its shape, the Archimedes screw is considered to be a fish-friendly turbine, as shown in research on fish migrations at a hydropower facility in Meinigem, Germany, conducted by Schmalz (2010).

The U.S. Corps of Army Engineers designed a new axial turbine rotor with fixed blades in 2016 to enhance the hydraulic guide channel for fish, and to replace one of the existing rotors at the Ice Harbor Dam in Washington State. Additionally, in 2017, three fish-friendly turbines, designed by DIVE Turbinen GmbH & Co. KG, were installed at a hydropower plant in Oeblitz, Germany, with a 3 × 300 kW capacity.

Hecker and Cook (2005), as cited by Ludewig et al. (2018), conducted a study to create a modified and

customized fish-friendly turbine (Alden VOITH type) for the Crescent hydropower generation facility, in Albany and Saratoga counties, with 12MW of generation capacity.

Despite progress in the development of new fish-friendly rotor geometries for high-power generation, few publicized methodologies exist for FTR turbine designs, though some of these designs are patent-registered. FTR designs have been emerging in research within the engineering field in recent decades as essential parts of the sustainable development of future hydropower projects. The importance lies in strong environmental and economic considerations (Odeh, 1999; Dixon & Dham, 2011; Hecker et al., 2012; U.S. Army Corps of Engineers, 2016; Oeblitz Hydroelectric Power Plant, 2017).

This study presents a methodology for drawing a hydraulic channel for the rotor to control pressure variation rates, the minimum absolute pressure, and strain rates induced by shear stresses. This creates a flow field that is consistent with the specifications previously defined for fish-friendly turbines. Furthermore, the aforementioned design methodology allows the rotor to be projected and integrated with optimization algorithms to enhance hydraulic efficiency without compromising the physiological integrity of the fish.

The significance of this study lies in proposing a specific turbine rotor design methodology aimed at achieving high hydraulic efficiency while ensuring fish survival. This accounts for parameters that promote fish survival rates when they pass through the turbine rotor, including the minimum absolute pressure, pressure variation rates, and the strain rate. The rotor is the most critical high-power generation component affecting fish survival rates, according to Čada (2001) and Loures (2012).

The added value and innovations presented in this study consist of an applied, parametrizable methodology for designing these types of turbine rotors, adaptable to all practical operation ranges needed for this technology, and which are capable of operating with high hydraulic efficiency. Simultaneously, the parametrization of the geometric control variables in this applied design methodology for fish-friendly turbine rotors allows any optimization technique to be implemented and turbine operational conditions to be customized to its design.

Design methodologies for fish-friendly turbine rotors have not been widely disseminated in the literature. This is attributed to existing patents and Non-Disclosure Agreements (NDAs) between various governmental agencies of several countries and private industry, as shown in Odeh (1999); Cook et al. (2000); Hecker and Cook (2005); Dixon and Dham (2011); Hecker et al. (2012), including U.S. Department of Energy partnerships with key private industries, e.g., Alden and Voith. Additionally, this applied methodology serves as a guide to researchers and designers who wish to delve into the research, development, and implementation of this type of turbine technology.

2. PRELIMINARY FISH-FRIENDLY ROTOR DESIGN

The project conditions specified by Dixon and Dham (2011) were considered for the preliminary rotor design, to obtain a comparison parameter for the hydraulic performance with the Alden Voith Turbine. The practical limits operation for the fish-friendly turbine design are shown in (Fig. 1), as per Dixon and Dham (2011), and are based on hydraulic head and volumetric flow data. The selected values for this design are as follows:

- $Q = 42.50\ m^3/s$
- $H = 31.11$ m
- $n = 120$ rpm
- $\eta_h = 0.90$ (η_l, η_{la}, $\eta_m \cong 1.0$),
- $u_4 = 24$ m/s (tangential velocity).

The magnitudes of n and u_4 match those from the Alden Turbine used in the pilot project at Brookfield Renewable's School Street Hydro Power Station, as proposed by Dixon and Dham (2011) and referenced by Nielsen et al. (2015).

Regarding the criteria for fish-friendly turbine designs, several parameters were considered:

- a minimum absolute pressure that influences rapid pressure drops and cavitation, at $p_{min} \geq 68$ kPa;
- a strain rate at $\epsilon = dv/ds \leq 180 s^{-1}$;
- and a pressure variation rate associated with flow turbulence through the turbine rotor, at $dp/ds \leq 550.3$ kPa/s.

These specifications were referenced by Odeh (1999), adopted by the Alden Research Laboratory and the Northern Research and Engineering Corporation, and align with those cited by Cooke et al. (2011).

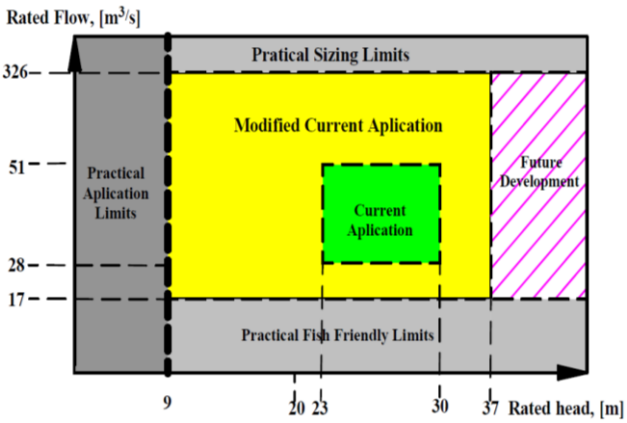

Fig. 1 Alden turbine application range. Adapted (Dixon & Dham, 2011)

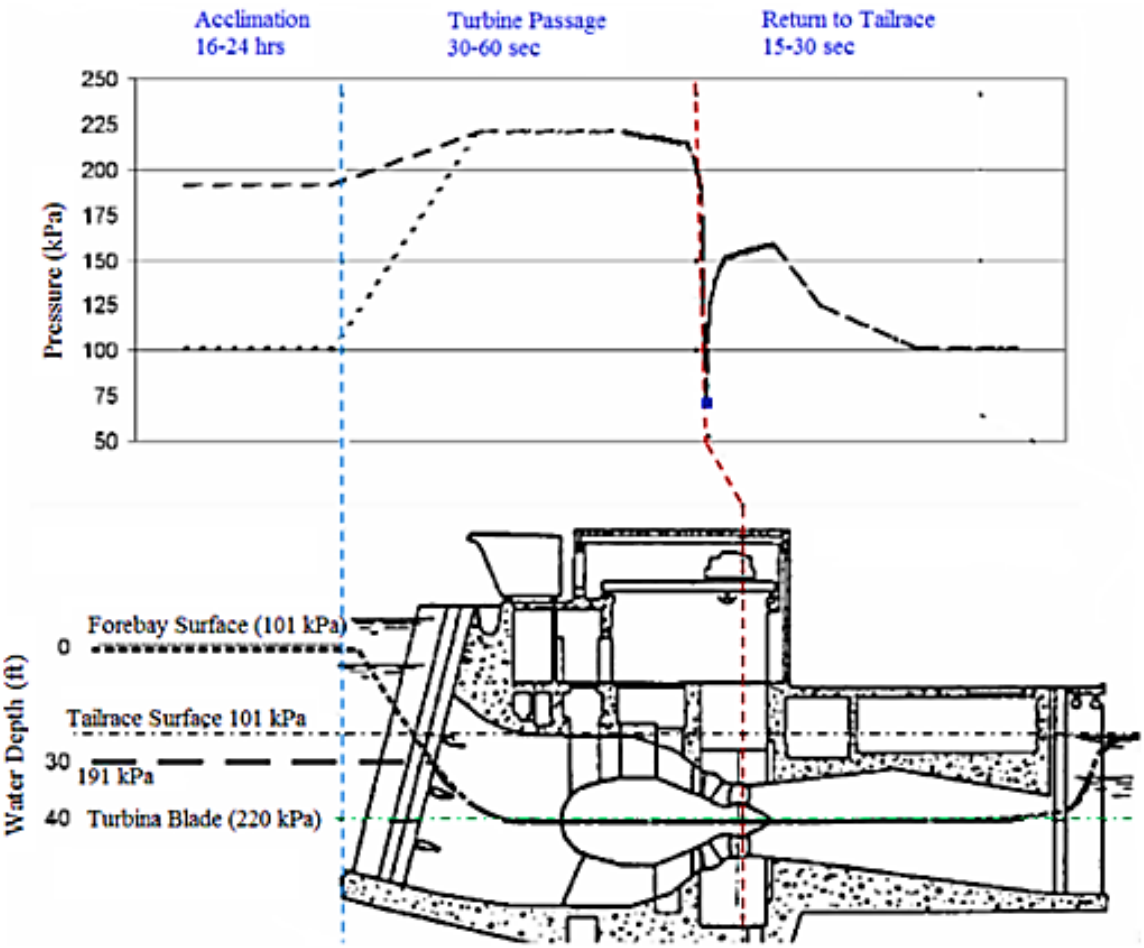

Fig. 2 Pressure and trajectory for a fish passing through the centerline of a Bulb Turbine. Figure adapted (Abernethy et al., 2002)

The term "fish-friendly" encompasses all the necessary physical flow conditions required to ensure fish survival. These criteria were generally determined, based on studies of several native North American fish species, and were mentioned in Odeh (1999). These criteria can be employed for Computational Fluid Dynamics (CFD) modeling. However, in specific situations, the response to injury mechanisms in the fish for a determined species must be evaluated with experimental data, considering factors like size variation, body shape, etc. (Hecker & Cook, 2005; Dixon & Dham, 2011; Cooke et al., 2011; Nielsen et al., 2015).

According to Abernethy et al. (2002) and Čada (2001), Fig. 2 shows two passage paths for fish approaching the bulb turbine rotor. In the acclimatization region, two pressures can be considered: one at the upstream surface (101 KPa) and another (191 KPa), corresponding to a depth of 30 feet. In this region, the fish are allowed an acclimation time of approximately 15 hours. Immediately upon entering the high-pressure piping, the absolute pressure values can reach approximately 225 kPa, within an average time of 45s. Finally, as the fish pass through the rotor, there is a pressure decrease, as low as 70 kPa (Abs), in only 0.1s. In the subsequent twenty seconds, the pressure rises to about 150 kPa in the draft tube and gradually decreases to 101 kPa in the tailrace (Fig. 2).

In Kaplan turbines, which are commonly used in hydroelectric dams, a similar pattern is seen. The most extreme pressure conditions occur at the intake region and near the blade tips. Peak pressures can reach as high as 340 kPa, and pressure can drop to as low as 2 kPa immediately after the rotor passes, as mentioned in Becker et al. (2003). The minimum absolute pressure experienced by the fish is referred to as Nadir's pressure, to which the fish are exposed for approximately 0.25 s. Immediately thereafter, the pressure rapidly recovers to atmospheric levels in the draft tube and tailwaters, as described by Watson (1995). Existing literature on the effects of pressure changes on fish is often specific in terms of species, location, and turbine design. The survival rate has been studied for species such as Lepomis macrochirus (Bluegill Sunfish), Juvenile Oncorhynchus tshawytscha (Fall Chinook Salmon), Oncorhynchus mykiss (Rainbow Trout), Gadus morhua (cod), and Pollachius Virens (saithe/coley).

Becker et al. (2003) experimentally simulated the pressure changes occurring during passage through a Kaplan turbine. In the acclimation region, pressures ranging between 101 kPa and 191 kPa can be encountered. In the inlet pipe, pressures increase to 400

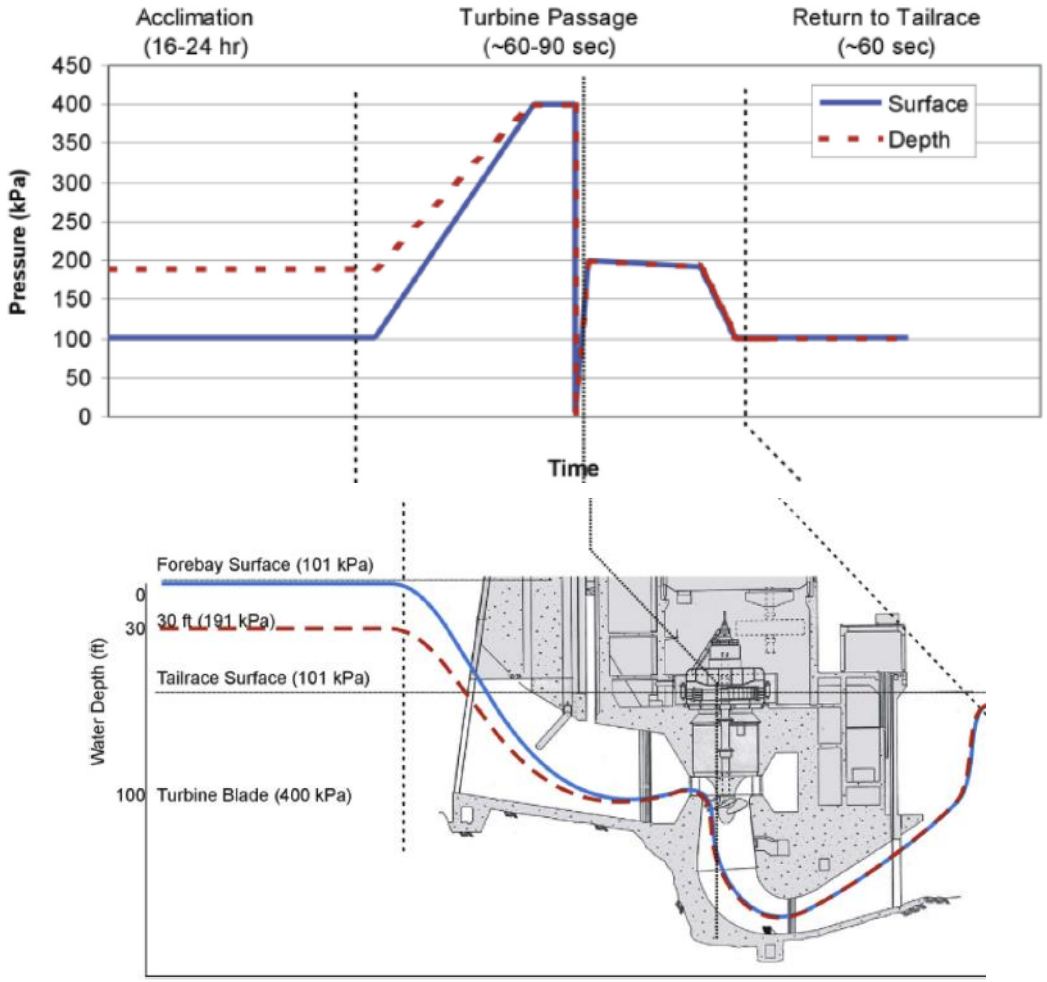

Fig. 3 Pressure exposure of turbine passage for surface and depth-acclimated fish for a Kaplan turbine. Figure adapted (Becker et al., 2003)

Table 1 Nadir's pressure at which mortality/injury appears to be negligible during a one-time exposure Becker et al. (2003)

Species	Death	Injury	Pressure drop
Bluegill Sunfish	~50 kPa*	> 50 kPa	350 kPa
Fall Chinook Salmon	2-10 kPa	2-10 kPa	390 – 398 kPa
Rainbow Trout	2-10 kPa	2-10 kPa	390 – 398 kPa

kPa within an average time of 45s. The fish are then exposed to a sudden pressure drop to 50 kPa within a time interval of 0.1s, and finally, they return to atmospheric pressure after exiting the draft tube. The pressure profile for the simulated turbine passage is shown in (Fig.3).

Becker et al. (2003) investigated the Chinook salmon, rainbow trout, and bluegill species. However, rainbow trout were not exposed to the most severe pressure changes, as described above. The fish were acclimated for 16 to 24 hours at starting pressures of 101 kPa or 192 kPa, corresponding to initial depths near the surface and 9.14 m (30 ft) from the surface, respectively. Resulting injuries included black spots on the top of the head, gas bubbles in the heart or in the afferent lamellar arteries of the gills, rupture or overinflation of the swimming bladder, and internal hemorrhaging near the swimming fins. All these effects proved fatal, with the ruptured swim bladder being the most common cause of death. At the Nadir pressure, mortality or injury appears to be negligible during a one-time exposure for each species listed in Table 1. For Bluegill, a Nadir higher than the reported 50 kPa is suggested, since injury rates at 50 kPa were significant.

3. ROTOR DESIGN METHODOLOGY

3.1 Determining the Rotor Dimensions

Considering the turbine rotor design parameters suggested by Odeh (1999) and cited by Cooke et al. (2011), the spaces between two consecutive blades should be made as large as possible, and the gap between the rotor components and the turbine shroud should be less than 2.0 mm to avoid injuring the fish. In this project, the number of blades matches the ALDEN VOITH turbine, with N_{blade}=3, and no clearance between the shroud and blades.

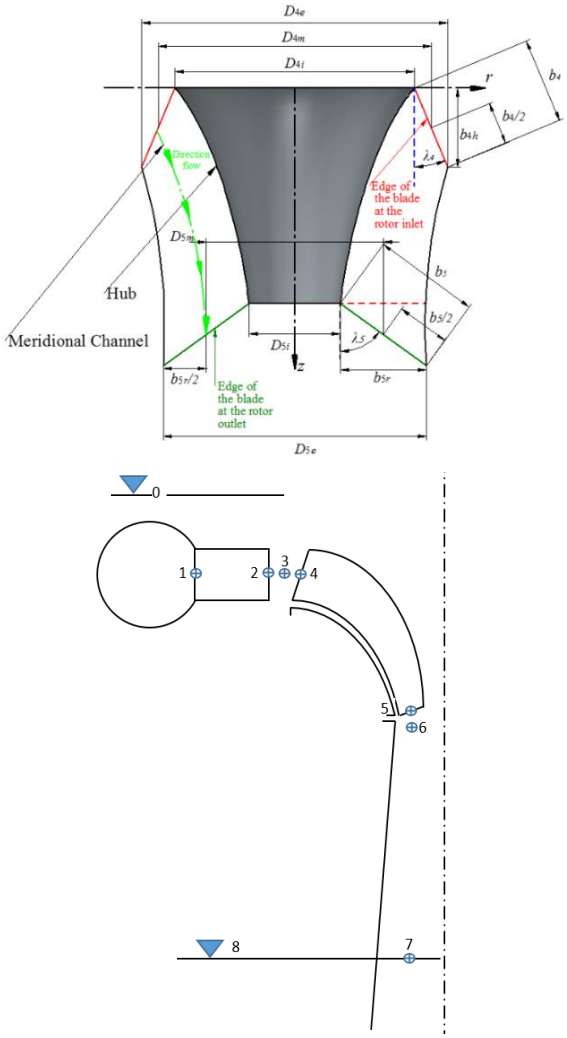

Fig. 4 General dimensions for the hub, leading and trailing edge at the rotor, and the reference points in the turbine

Additionally, the chosen configuration for the number of blades, N_{blade}=3, was based on the results obtained by Odeh (1999), where it was demonstrated that the three-blade rotor showed the best global efficiency relative to rotors with one and two blades.

On the other hand, increasing the blade number to four enhances the probability of mortality by 25% due to blade strike injuries, irrespective of the species and size of the fish, according to the probability equation for mortality resulting from blade strike injuries, as per Hecker et al. (2012). Therefore, in the rotor design, the shroud was fixed to the blades, and the hydraulic channel size was maximized. This configuration eliminates gaps between moving and fixed parts, thus preventing the fish from being injured or crushed.

The characteristic dimensions of the turbine rotor in the meridional plane, as seen in (Fig. 4), were determined based on the specific rotation, calculated according to the Addison formulation, n_{qA}, Eq. (1).

$$n_{qA} = n\frac{Q^{1/2}}{Y^{3/4}}10^3 \tag{1}$$

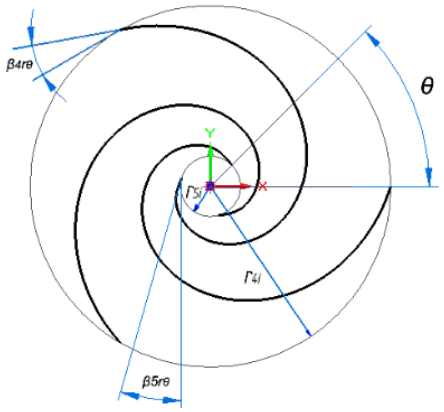

Fig. 5 Angles $\beta_{4r\theta}$ and $\beta_{5r\theta}$ at the blade drawing

It is important to note that the preliminary design of turbomachinery is based on the dimensionless relationships that define the geometric characteristics of hydraulic turbines. In this study, these relationships will be presented and discussed, considering n_{qA} = 193 based on the design conditions (n=120 rpm, Q=42.5 m^3/s, and H=28 m).

The basic dimensions of the rotor are determined at the beginning of this methodology by accounting for the peripheral or tangential velocity at the rotor inlet u_4=24 m/s, resulting in a Medium Inlet Diameter of D_{4m}=3.82 m.

The following relationship is established for diameter D_{4i}: $D_{4i}=u_{4i}/\pi n$. The diameter ratio $k_1=D_{4i}/D_{5i}$ is determined by the sweep angle of the blade θ at the spiral with a linear $\beta_{r\theta}$ angle variation. The k_1 value was established iteratively, and this k_1 value defines the value of D_{5i}. θ = 180° was chosen for the Preliminary Design of the Turbine Rotor Geometry, as shown in (Fig.5). Then, the D_{4i} value is used to first estimate the outlet diameter of the rotor D_{5e}/D_{4i}.=0.9.

The parameters for determining the k_1 values, representing the ratio D_{4i}/D_{5i}, will be shown in the Blade Geometry Generation section.

Based on the geometric relations for Francis Turbine rotors, one can calculate the width of the blade b, as shown in (Fig. 6), where the blade width is either a radial component at the rotor inlet $b_{4h,}$ or an axial component at the rotor outlet b_{5r}, considering that $b=b_{4h}=b_{5r}$. The blade width b is then ascertained using the previously established specific rotation and the ratio k_2=10 (b/D_{5e}.).

The D_{5e} value is calculated with the blade width b; however, this value must replace the initial estimation (D_{5e}/D_{4i}.=0.9). Therefore, a correction for D_{5e} is expressed by the equation $D_{5e}=2b_{5r}+D_{5i}$. Once the blade width b is determined, and the outlet external diameter of the rotor D_{5e} is updated, other dimensions of the rotor, like the blade width at the inlet and the outlet, are then calculated.

Due to differences in the blade width at the rotor inlet b_4, and the rotor outlet b_5, when the opening blade

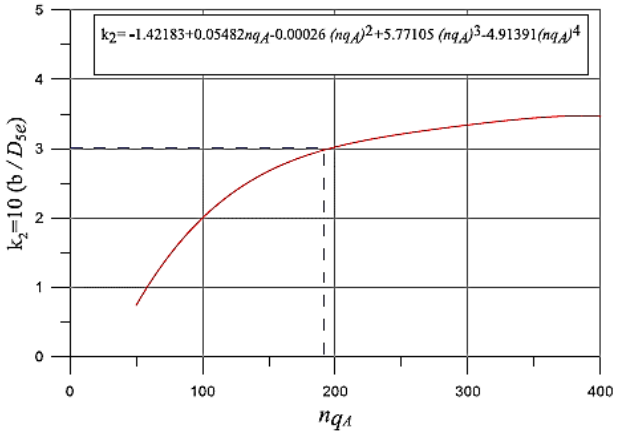

Fig. 6 Elements of the preliminary design for a Francis rotor. Figure adapted (Bran & de Souza, 1969)

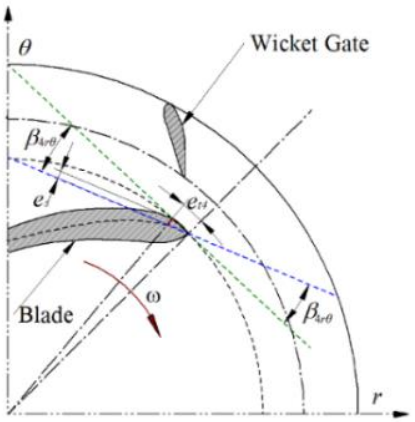

Fig. 8 Approximate blade tangential thickness at the inlet rotor, plane [r, θ]

angle λ_5 is not equal to 90°, the blade width is determined by a linear increment Δb between b_4 and b_5 along the blade path. This leads to variations in the width of the leading and trailing edge at the channel, as shown in (Fig. 4).

3.2 Flow at the Rotor Inlet

A representative trajectory of the flow at the mid-height of the blade from the rotor inlet to the rotor outlet was considered for the analysis of the rotor flow, assuming a finite number of blades, where the meridional component was calculated in terms of the volumetric flow of the rotor, Q.

A Distributor system with an infinite number of blades was considered, where the volumetric flow is perfectly directed to the rotor inlet, as depicted in (Fig. 7). This results in meridional velocity components C_{m4}, relative velocity w_4, and tangential velocity at the rotor inlet, u_4. We should emphasize that in this study, and throughout the following sections and discussions, the inlet and outlet velocity triangles are referenced to the streamline at the mid-height of the blade. Consequently, by knowing the area at the rotor inlet (($A_4=\pi D_{4m}b_4$), the volumetric flow of the rotor, Q, and the obstruction

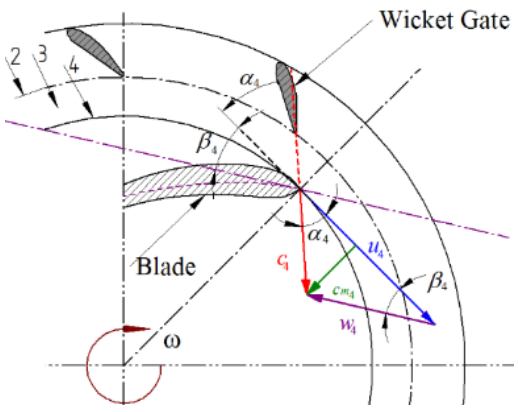

Fig. 7 Velocity triangle at the upper plane (inlet)

factor at the rotor inlet, f_{e4}, the meridional velocity at the mid-height of the blade at the rotor inlet can be determined. See Eq. (2).

$$c_{m3}=\frac{Q}{A_4\, f_{e4}}\ ;\ c_{m4}=\frac{Q}{\pi D_{4m} b_4 f_{e_4}};\ D_{4m}=\frac{D_{4e}+D_{5i}}{2} \tag{2}$$

The obstruction factor, f_{e4}, results from a flow reduction when considering a finite number of blades in the rotor, each with a finite thickness. In this study, obstruction factors, f_{e4}, were analyzed via their geometric relationships, evaluating the shape of the leading edges of the hydrofoils used in a subsequent optimization process via DOE: Goe 622, Goe 408, and Goe 474. See Eq. (3) and (Fig. 8).

$$e_{t_4}\approx\frac{e_s L_{mp}}{\sin\beta_{4r\theta}};\ t_4=\frac{\pi D_{4m}}{N_{Blade}};\ fe_4=\frac{\left(t_4-e_{t_4}\right)}{t_4} \tag{3}$$

Principally, the type of hydrofoil and the sweep angle of the blade, θ, used in each rotor geometry generation influence the obstruction factor value at the inlet, f_{e4}. The range of f_{e4} values obtained through this procedure was between 0.91 and 0.95, considering the range of blade sweep angles, θ, and hydrofoils used in all stages of this study.

To determine the term e_{t4}, blade thickness, e_s, was taken as being 1.25% of the chord length of the chosen hydrofoil. This 1.25% factor of the cord length of the hydrofoil is generally the nearest discretization point with respect to the initial discretization point of the tabulated hydrofoils or airfoils. See (Fig. 9).

The velocity triangle configuration at the rotor inlet is based on the velocity vector composition $c_4=u_4+w_4$, which considers a finite number of blades without shocks, see (Fig. 7) and (Fig. 10(a-b)), considering the assumption of the meridional mean velocity configuration at the rotor inlet $c_{m3}\approx c_{m4}$. On the other hand, it highlights that the velocity triangle at the rotor inlet has axial components for velocities c_4, c_{m4}, and w_4, given the blade angle λ_4. Therefore, a cylindrical coordinate system was adopted to determine the compositions of the velocities, considering the directions in planes [r, z] and [r,θ]. See (Fig. 10 (a-b)).

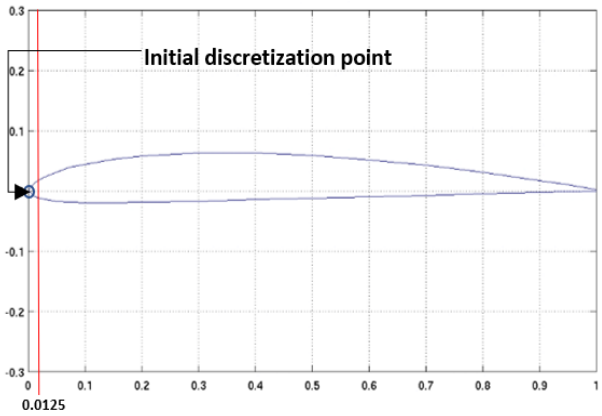

Fig. 9 Percentage Discretization of the hydrofoils along the cord length. Figure adapted. UIUC Airfoil Data Site

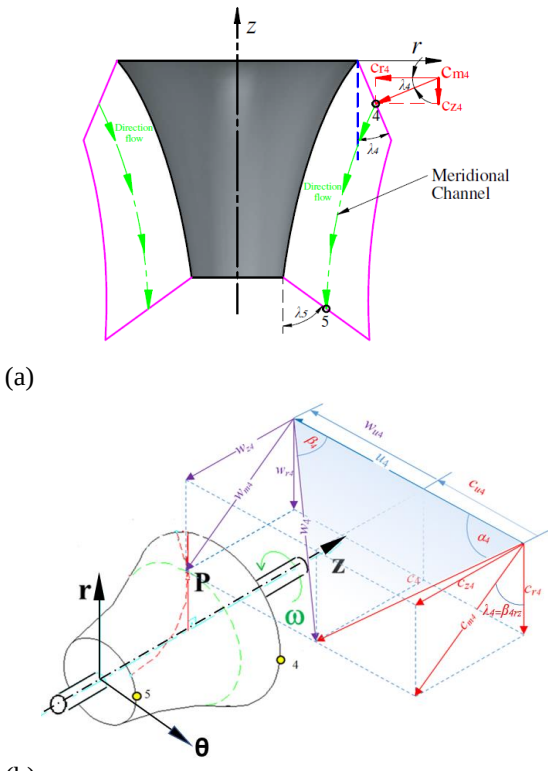

(a)

(b)

Fig. 10 (a) Meridional velocity components at the meridional plane. (b) Velocity triangle configuration at the rotor inlet in cylindrical coordinates

3.3 Hub Geometry Generation

To generate the cube, a smoothed conical shape, given by a second-order polynomial curve, was used. This particular type of curve was employed to obtain a more favorable distribution of the pressure gradient along the channel. Mathematical functions, through variations in their coefficients, allow geometric modifications to be generated that are controlled by optimization processes.

The drawing for the hub is defined by the intersection of two straight lines on the plane [*r*, *z*], based on angles δ and γ and points (r_{4i}, 0) and (r_{5i} , -*h*), see (Fig. 11), where the intersection is defined by points (r_{int} , z_{int}), as shown in Eq.(4) and Eq.(5).

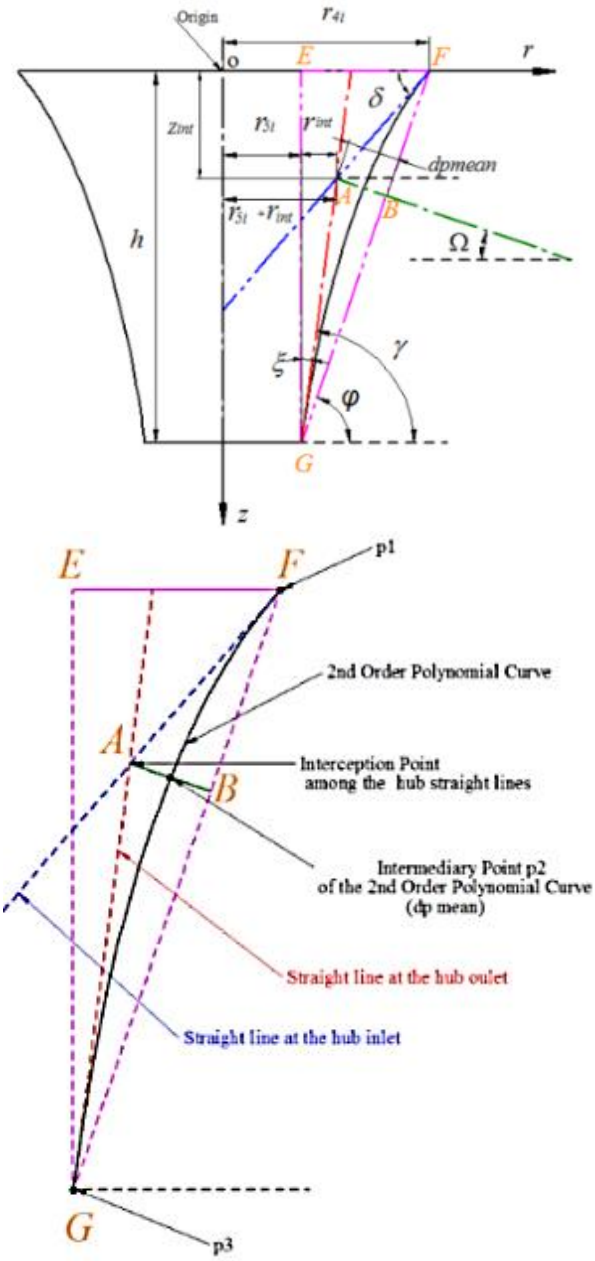

Fig. 11 Construction of the hub geometry in the plane [r, z]

$$r_{\text{int}} = \frac{r_{5i}\tan\delta\tan\xi - (r_{4i}\tan\delta\tan\xi + h\tan\xi)}{1-\tan\delta\tan\xi} \tag{4}$$

$$z_{\text{int}} = (r_{\text{int}} + r_{5i} - r_{4i})\tan\delta \tag{5}$$

Where the angle restrictions for δ, γ, and φ for the hub drawing are $\gamma<90°$, $\gamma>\delta$, and $\gamma\geq\varphi$. The hub shape is generated via the trajectory of a second-order polynomial through points $P_1(r_{4i},0)$, an intermediary point $P_2(r_{5i}+r_{int}+dp_{mean\ r}, -z_{int}-dp_{mean\ z})$, and $P_3(r_{5i}, h)$, where dp_{mean} is formed from the intersection point and the line that passes through the intersection point which is perpendicular to segment *FG*. See Eq. (6).

$$z = f(r) = a_o + a_1 r + a_2 r^2 \tag{6}$$

dp_{mean} is defined as a fraction of the length of segment d_{AB}, where $dp_{mean}=c(AB)$. The geometric parameter *c* intervenes and shapes the hub, rendering it more

pronounced or smoother, directly influencing the volumetric flow that passes through the rotor.

This method for hub generation, based on parameter *c*, allows a new hub profile geometry to be configured. Using a Vandermonde matrix, a linear system of equations is solved to obtain the constants (a_0, a_1, a_2), as shown in Eq. (7).

$$\begin{bmatrix} 1 & r_{4m} & r_{4m}^{\,2} \\ 1 & \left(r_{5i}+r_{int}+dp_{mean}\right) & \left(r_{5i}+r_{int}+dp_{mean}\right)^2 \\ 1 & r_{5i} & r_{5i}^{\,2} \end{bmatrix} \begin{Bmatrix} a_0 \\ a_1 \\ a_2 \end{Bmatrix} = \begin{Bmatrix} 0 \\ -z_{int}-dp_{mean} \\ -h \end{Bmatrix} \quad (7)$$

Coefficients (a_0, a_1, a_2) may be optimized in accordance with other variables defined in the rotor, e.g, the hydrofoil and the hub construction angles.

3.4 Blade Geometry Generation

A spiral function incorporating a linear variation in the relative flow angle $\beta_{r\theta}$ was employed to generate the blade geometry in the plane $[r,\theta]$. This approach is commonly used when designing centrifugal turbomachinery (Srinivasan, 2008; Hou et al., 2016). See (Fig. 5) and Eq. (8) for additional details.

$$r(\theta) = -\frac{r_{4i}k_4}{\tan\beta_{4r\theta}\, e^{-k_4\theta} - r_{4i}k_3} \quad (8)$$

Where constants k_3 and k_4 are obtained based on the relative flow angles $\beta_{4r\theta}$ and $\beta_{5r\theta}$ (at the leading edge and the trailing edge, respectively) and the hub radius at the rotor inlet and outlet, r_{4i}, and r_{5i}, respectively. See Eq. (9) and Eq. (10).

$$k_3 = \frac{\tan\beta_{4r\theta} - \tan\beta_{5r\theta}}{r_{4i} - r_{5i}} \quad (9)$$

$$k_4 = \tan\beta_{4r\theta} - \frac{r_{4i}\left(\tan\beta_{4r\theta} - \tan\beta_{5r\theta}\right)}{r_{4i} - r_{5i}} \quad (10)$$

In Equations (10) and (11), one can see that if angle $\beta_{4r\theta}$ remains constant along the path, a logarithmic spiral is defined by the inlet and outlet angles in the rotor. Point spatial discretization was employed using a vector approach for the blade projection.

Regarding determining k_1, which represents the ratio D_{4i}/D_{5i}, and recognizing that r_{4i} and the desired sweep angle of the blade θ are both known, an iterative process can be performed to obtain r_{5i}. This value must satisfy the imposed input θ value via Eq. (11).

$$\theta_{max} = -\frac{1}{k_4}\left(ln\left(\frac{r_{4i}\tan\beta_{4r\theta}}{r_{5i}\tan\beta_{5r\theta}}\right)\right) \quad (11)$$

3.5 Mean Absolute Outlet Flow Angle Correction at the Mid-blade

Another significant consideration in the design of the turbine rotor is flow correction, to secure the axial direction of the absolute velocity at the outlet, resulting in maximum specific energy (hydraulic energy). Thus,

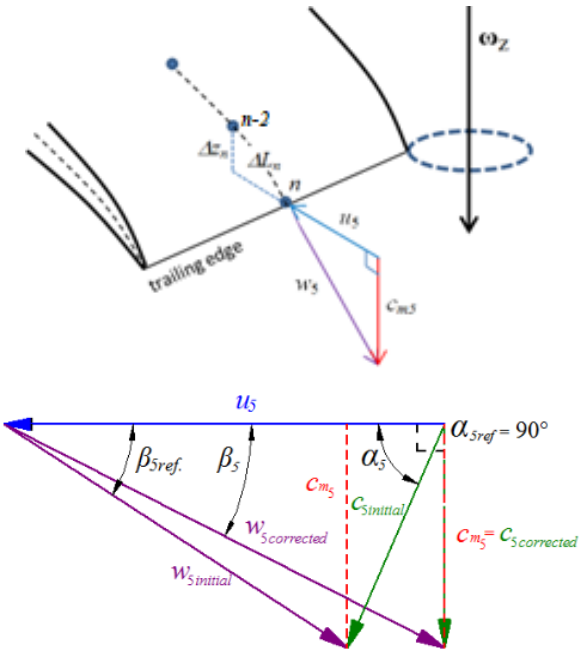

Fig. 12 Initial and corrected velocity triangle configuration at the rotor outlet in the meridional plane, for an axial outflow

the preliminary design considers the tangential component of the absolute velocity at the rotor outlet, c_{u5}=0. This correction was performed at the mid-blade width at the rotor outlet, considering angle α5, where the rotor outlet area is defined as an annular area. Therefore, when the rotor has few blades, and when the obstruction factor is approximately equal to one, the meridional mean velocity at the rotor outlet can be defined as:

$$c_{m5} = \frac{Q_{Rotor}}{\pi D_{5m} b_{r5} f_{e5}};\; D_{5m} = \left(\frac{D_{5e}+D_{5i}}{2}\right);\; b_{5r} = \left(\frac{D_{5e}-D_{5i}}{2}\right) \quad (12)$$

The velocity triangle at the rotor outlet is calculated at the mid-blade, where the flow angle $\alpha_{5ref} \neq 90°$ is initially not equal to 90°. The Δz_n component, as shown in (Fig. 12), must be iterated until it is perpendicular to $\alpha_{5\text{-}corr}$ = 90°. This correction greatly enhances the specific energy extracted by the rotor. One requirement is that $\alpha_5 = \alpha_{5ref}$ =90° and $c_5 = c_{m5}$ to correct the absolute flow angle at the mid-blade width in the rotor outlet. The *n-2* discretization point was chosen to provide a smoother angle correction. By contrast, the velocity triangle at the rotor outlet, without correcting the absolute angle of the flow at the mid-blade width, is established in the meridional plane. Thus, the absolute mean velocity in the meridional plane, $c_{5\ initial}$, will differ from the desired condition α_5 =90° for the meridional mean velocity at the rotor outlet, c_{m5}, for generating an axial outflow at the mid-blade. See (Fig. 12).

Subsequently, an iterative correction over angle β_5 was necessary, achieved by varying the rotor height until it satisfied the condition where $\beta_5 = \beta_{5ref}$. By performing this correction, the meridional mean velocity magnitude at the rotor outlet will be equal to the corrected magnitude of the mean absolute velocity at the rotor outlet, in the mid-blade $c_{m5} = c_{5corrected}$.

The design conditions pertaining to the volumetric flow Q, head height H, rotation n, and tangential velocity at the rotor inlet u_{4ref} were accounted for in the iterative process, along with previously determined geometric variables like $\beta_{4r\theta}$, $\beta_{5r\theta}$, λ_4, λ_5, θ, γ, and δ. From these considerations, the basic dimensions of the rotor, including the diameters, blade widths, and other variables (D_{4i}, D_{5i}, b, b_4, b_5, D_{5e}, D_{4m}, D_{4e}, D_{5m}) were all calculated. Thus, the iterative process starts with an initial rotor height value. Using these data, the geometry of the blade is discretized, and subsequently, the velocity at the rotor output c_{m5} and angle β_5 are both computed. The calculated angle β_5 is compared to the reference angle β_{5ref}, and if both angles align, the process concludes. If the angles differ, however, the rotor height is adjusted, and the iterative process restarts until converging (Niño Del Río, 2018).

The correction of the angle over the outlet flow at the mid-blade enhances the hydraulic performance of the turbine rotor and reduced the turbulence levels that fish are exposed to at the rotor outlet.

The previous parametrizations described for generating the hub and blade, as well as the current Mean Absolute Outlet Flow Angle Correction procedure at the

Mid-blade, can be employed as a unified set for applying an optimization methodology, as used in Silva et al. (2012). The application of this optimization methodology would involve enhancing the hydraulic performance of the turbine through integrations with optimization probabilistic algorithms and using response surface constructions to streamline the search process for maximum hydraulic efficiency. This would be done while also accounting for fish-friendly parameters, e.g., lateral restrictions or limitations that would ensure fish survival.

3.6 Draft Tube

A modified geometry was selected for the draft tube, derived from the original geometry of a GAMM Francis turbine (*Gesellschaft für Angewandte Mathematik und Mechanik* - Applied Mathematical and Mechanics Society), and optimized by modifying the elbow generatrix curve in a hyperbolic format, as per Arispe et al. (2016) and Arispe et al. (2018). See Fig. 13. This geometry employed the minimum loss coefficient value in the CFD simulations conducted by Arispe et al. (2016) and Arispe et al. (2018) for the GAMM Francis turbine.

To integrate the turbine rotor and draft tube geometries, a conical transition section was fashioned with an opening angle at 6º, as recommended by Macintyre (1987), and a height of 1 m. Using a draft tube with a cross-section transitioning from circular to square is recommended to decrease loss coefficients and enhance the efficiency of the fish-friendly turbine. It is worth noting that better-optimized configurations for draft tubes, as used by Dixon and Dham (2011) when developing the ALDEN-VOITH Fish Friendly Turbine,

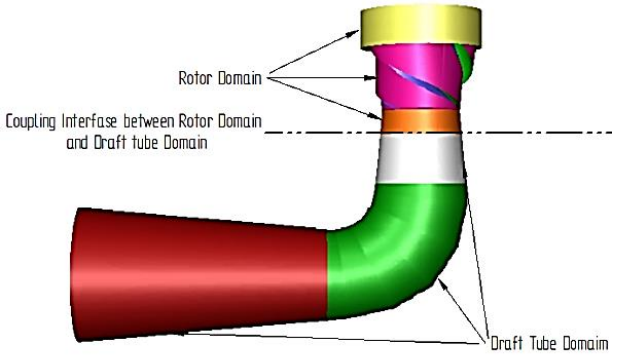

Fig. 13 Draft tube projected with a hyperbolic generatrix curve at the elbow coupled with a fish-friendly rotor geometry

are available; however, the focus this study is on the development of a Methodology for designing the rotor.

3.7 Turbine Geometry Generation

First, a Preliminary Design (PD) of the turbine rotor geometry was established, along with the geometric variables, thus starting an adjustment process to identify the values of the geometrical variables. This was done via a previously conducted sensitivity analysis to arrive at a base configuration with an acceptable hydraulic efficiency, corresponding to the volumetric flow at the turbine's design operation point. The outcome of the adjustment process was the Base Design (BD) turbine rotor geometry, which reached an acceptable hydraulic efficiency concerning the volumetric flow at the design operation point of the turbine, Q =42.5 m^3/s.

The PD turbine rotor geometry, the BD turbine rotor geometry, and additional rotor geometries used in the DOE were generated using commands in the Tcl/Tk computational language through scripts tailored for interpretation by ICEM CFD®, as shown in (Fig. 14). The geometrical parameters chosen for creating the PD turbine rotor geometry are shown in Tables 2 and 3, and the parameters selected for generating the BD turbine rotor geometry are shown in Tables 4 and 5.

Geometric parameter c=0.3 was used to generate the hub for the PD turbine rotor geometry, while the BD turbine rotor geometry and the Optimized Geometry (OG) turbine rotor used c=0.7.

Göttingen family hydrofoils have been widely employed in hydraulic machine design like Francis and Kaplan turbines, showing maximum efficiency values as described in Vivier (1966). However, we should emphasize that any type of hydrofoil with currently used optimized geometries could be integrated into the aforementioned blade rotor generation methodology.

4. NUMERICAL APPROACH

4.1. Governing Equations

The Governing Equations used in the numerical simulations were the RANS (Reynolds Average Navier

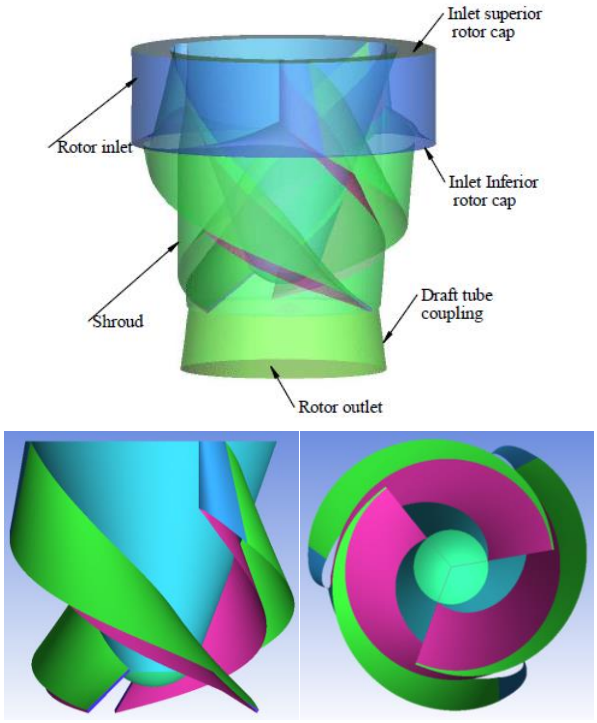

Fig. 14 Rotor domain components and views

Table 2 Variables of the PD turbine rotor geometry

Blade width [m]	Hub angles [°]	θ [°]	β angles [°]	Hydro foil	λ angles [°]	N_{blade}
b_4= 1.026 b_5= 1.057	δ=47 γ=78	180	$\beta_{4r\theta}$=18 $\beta_{5r\theta}$=18	Goe 622	λ_4=0.5 λ_5=76	3

Table 3 Parameters of the PD turbine rotor geometry

D_{4i} [m]	D_{4m} [m]	D_{4e} [m]	D_{5i} [m]	D_{5m} [m]	D_{5e} [m]	h_{hub} [m]
3.812	3.821	3.83	1.245	2.271	3.297	2.227

Table 4 Variables of the BD turbine rotor geometry

Blade width [m]	Hub angles [°]	θ [°]	β angles [°]	Hydro foil	λ angles [°]	N_{blade}
b_4=1.012 b_5=1.190	δ=70 γ=89	180	$\beta_{4r\theta}$=19 $\beta_{5r\theta}$=20	Goe 622	λ_4=4.5 λ_5=58	3

Table 5 Parameters of the BD turbine rotor geometry

D_{4i} [m]	D_{4m} [m]	D_{4e} [m]	D_{5i} [m]	D_{5m} [m]	D_{5e} [m]	h_{hub} [m]
3.748	3.827	3.907	1.162	2.171	3.180	3.729

Stokes) equations, which are suitable for describing a steady regime where the flow behavior properties in the local flow field depend solely on spatial conditions. These spatial conditions are determined via the domain through which the flow passes, independent of temporal conditions. Eq. (13) corresponds to the Continuity equation, and Eq. (14) corresponds to the Momentum conservation equation. Both equations articulate differential formulations.

$$0 = \frac{\partial \bar{\rho}}{\partial t} + \frac{\partial \bar{\rho}\tilde{u}_i}{\partial x_i} \tag{13}$$

$$\frac{\partial \bar{\rho}\tilde{u}_i}{\partial t} + \frac{\partial \bar{\rho}\tilde{u}_i\tilde{u}_j}{\partial x_j} = -\frac{\partial \overline{\rho u_i'' u_j''}}{\partial x_j} - \frac{\partial \bar{p}}{\partial x_i} + \frac{\partial \overline{2\mu\left(S_{ij} - \frac{1}{3}\delta_{ij}S_{ii}\right)}}{\partial x_j} \tag{14}$$

Given the isothermal nature of the flow's physics in the numerical simulations, there was no need to include the Energy equation in our application.

4.2. Turbulence Model

The numerical simulations were conducted using the ANSYS Fluent® software program. The turbulence model was the k-ω SST (Shear Stress Transport) model comprising two equations, as described by Menter et al. (2003), presented in Eq. (15). Simultaneously, Newtonian, viscous, and isothermal flows were considered in a steady state, employing the multi-reference frame approach. The k-ω SST model of two transport equations is frequently used in wall-bounded or internal flows, where significant adverse pressure gradients exist. This turbulence model exhibits improved accuracy relative to other two-equation turbulence models (like the standard k-ε, RNG and Realizable k-ε, and k-ω models) with respect to experimentally corroborated data, as per Bardina et al. (1997), cited in Dixon and Dham (2011).

$$\begin{aligned} \frac{D\rho k}{Dt} &= \tau_{ij}\frac{\partial u_i}{\partial x_j} - \beta^* \rho\omega k + \frac{\partial}{\partial x_j}\left[\left(\mu + \sigma_k \mu_t\right)\frac{\partial k}{\partial x_j}\right] \\ \frac{D\rho\omega}{Dt} &= \frac{\gamma}{\nu_t}\tau_{ij}\frac{\partial u_i}{\partial x_j} - \beta\rho\omega^2 + \frac{\partial}{\partial x_j}\left[\left(\mu + \sigma_\omega \mu_t\right)\frac{\partial \omega}{\partial x_j}\right] \\ &+2\left(1-F_1\right)\rho\sigma_{\omega 2}\frac{1}{\omega}\frac{\partial k}{\partial x_j}\frac{\partial \omega}{\partial x_j} \end{aligned} \tag{15}$$

The k-ω SST model employs the k-ω formulation in the inner regions of the boundary layer and selectively and automatically, switches to the k-ε formulation for the outer part of the boundary layer through blending functions, as described in Menter et al. (2003). Additionally, the k-ω SST model shows lower turbulence levels than those in the k-ε model in high stagnation regions, in the presence of significant velocity gradients, and at the leading and trailing edges of the blades, as per Dixon and Dham (2011).

Menter et al. (2003), state that the k-ω SST turbulence model is a two-equation eddy-viscosity model that has substantially increased in popularity. Using a k- ω formulation in the inner parts of the boundary layer allows the model to be directly applied all the way to the wall through the viscous sub-layer, making the k-ω SST model suitable as a Low-Re turbulence model without requiring additional damping functions. The SST

Table 6 Determining the suction height in the PD turbine geometry

b_{4h} [m]	h_{Dr} [m]	h_{Drn} [m]	$h_{Draft\ tube}$ [m]	h_{water} [m]	p_7 [Pa]
1.026	3.482	2.969	6.028	9.51	88080.13

Table 7 Determining the suction height in the BD turbine geometry

b_{4h} [m]	h_{Dr} [m]	h_{Drn} [m]	$h_{Draft\ tube}$ [m]	h_{water} [m]	p_7 [Pa]
1.009	5.12	4.62	5.82	10.44	102,293.4

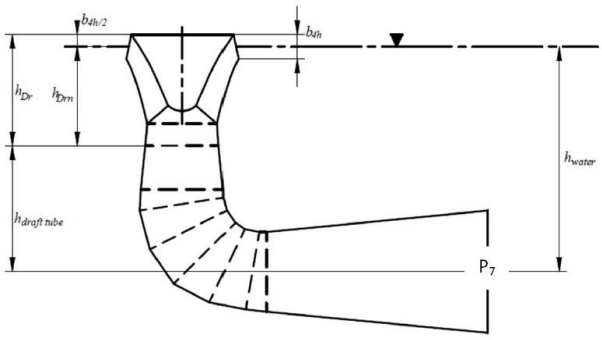

Fig. 15 Turbine configuration for determining the outlet Pressure

formulation also transitions to k-ε behavior in the free stream, thus avoiding the common k-ω problem where the model is overly sensitive to the inlet free-stream turbulence properties. Authors who employ the k-ω SST model frequently speak highly of it, given its favorable performance in adverse pressure gradients and in separating flows.

4.3. Boundary Conditions and the Numerical Scheme

With regard to the established boundary conditions, both incompressible flow and steady-state were considered, along with the following dynamic viscosity and water density values, measured at 20°C, which is a common temperature for Brazilian fish in their natural habitats: μ=1.003×10^{-3} Pa-s and ρ=998 kg/m^3, respectively. For the numerical simulation, gravitational acceleration was 9.81 m/s^2. Since the temperature change is negligible, an isothermal flow behavior was assumed, and the use of the energy equation was deemed unnecessary.

The inlet boundary condition was defined by the absolute mean velocity at the tangential, radial, and axial components, as established by the preliminary rotor design. This design ensures that the relative velocity flow aligns perfectly with the blade, enabling the meridional velocity to enter perpendicularly to the rotor inlet surface. Additionally, the pressure at the rotor inlet was determined as the static pressure corresponding to the project net head height H=28 m (274,130.64 Pa). It should be noted that the guide vane system was not modeled; instead, an assumption was made that the absolute velocity incident upon the rotor was equal in both magnitude and direction to that exiting the guide vanes. This simplification reduces the computational power that would be otherwise needed, which is especially significant when employing an iterative optimization process.

Static pressure (outlet pressure) at the draft tube outlet was established for the geometries, determined according to the respective rotor and draft tube domain heights. The pressure at the draft tube outlet for the Preliminary Design Turbine geometry was set at 88080.13 Pa, and for the Base Design Turbine Geometry, it was set at 102,293.40 Pa, as shown in Table 6 and Table 7, respectively (see Fig. 15).

Two domains were considered when configuring the turbine for the numerical simulations: one non-inertial (rotor domain), and another inertial (the draft tube) domain. The shroud and rotor inlet caps were designed to rotate in unison with the rotor components, leaving no gap between the shroud and the blade tips. Concurrently, the rotating walls of the rotor domain were defined under nonslip conditions. An interface was employed to couple the rotor domain and the draft tube domain, along with the rotor outlet domain and the inlet at the draft tube, and to ensure a steady state, the velocities for each domain in this region are identical. The turbulence intensity at the rotor inlet and the draft tube outlet was set at a typical value for turbomachinery, at approximately 5%, and the hydraulic diameter was also taken into consideration.

The SIMPLES numerical scheme was used for the numerical simulations. Regarding the Interpolation Schemes employed in the spatial discretization: the Standard Method was applied for the Moment; Upwind Second Order Schemes were used for the Turbulent Kinetic Energy k and the Specific Dissipation Rate ω.

4.4. Computational Mesh and Mesh Independence Analysis

A hybrid mesh was generated within the rotor for the BD turbine geometry, consisting of 10 prismatic layers and a hexahedral core, with a total of 9,726,188 cells, referred to as the reference mesh M_{ref} (Fig. 15 a-b). Additionally, a structured mesh containing 1,792,280 cells was created for the draft tube geometry. In the mesh independence analysis, consideration was given solely to the rotor domain. For this analysis, a second, more refined mesh was created on the rotor with 16,865,925 cells, named M_{high}, while maintaining the number of elements in the draft tube, as examined and validated by Arispe et al. (2018). Figure 16 a-b shows the mesh structure with 9,726,188 elements in both the transverse and longitudinal planes. The Independence Mesh Criterion applied was the percentual variation between the variables evaluated, i.e., the hydraulic efficiency and the moment, which must not exceed 1%, considering both the reference mesh and the high-refined mesh, as defined by LEAP CFD TEAM (2012). Concurrently, various authors have employed these criteria to confirm the independence of the results from the mesh used in the

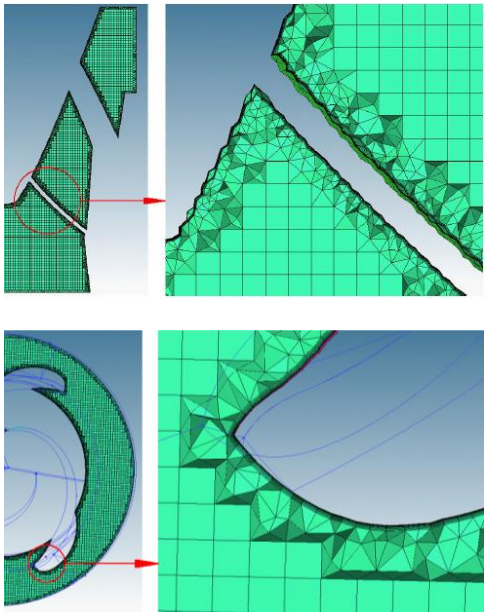

(a)

(b)

Fig. 16 (a) Detail of the front view cut of the rotor, M_{ref}. and (b) detail of the upper view cut of the rotor, M_{ref}

Table 8 Mesh independence analysis

Mesh	Size (cell number)	Hydraulic Efficiency at Q=27m^3/s [%]	Moment [N-m]
M_{ref}	9,726,188	88.15	1.789,766.9
M_{high}	16,865,925	88.08	1,780,983.3
Percentage Variation		0.49%	0.07%

numerical simulations (e.g., Aguirre et al., 2019); Arispe et al. (2018), among others).

The percentage differences in the hydraulic efficiency and moment results, based on the volumetric flow condition of the rotor (Q=27.0 m³/s), were applied as mesh independence criteria. These parameters vary by less than 1% between M_{ref} (initial reference mesh) and M_{high} (refined mesh), as shown in Table 8. Having confirmed the mesh independence of the numerical simulation, the reference mesh M_{ref} was selected for subsequent analysis.

The distribution of y^+ values within the rotor domain, including the blades, ogive, and hub, is shown for a volumetric flow at Q=27 m³/s, where the turbine's maximum hydraulic efficiency is achieved (see Fig. 17 a). One can see that within the zones of interest that were previously identified (namely the blades' walls, hub's walls, and ogive's walls), the maximum y+ values fall within the intermediary layer in a range of 0–140. This range represents 99.88% of the values calculated for the blades, and 99.99% for the hub and ogive. Figure 17 b gives a bar graph, where the variation of y^+ between 40 and 90 appears more frequently on the surfaces of the blades, the hub, and the ogive.

Other geometries derived from the DOE, similar to the optimization process, also adhered to the same general parameters of the reference mesh.

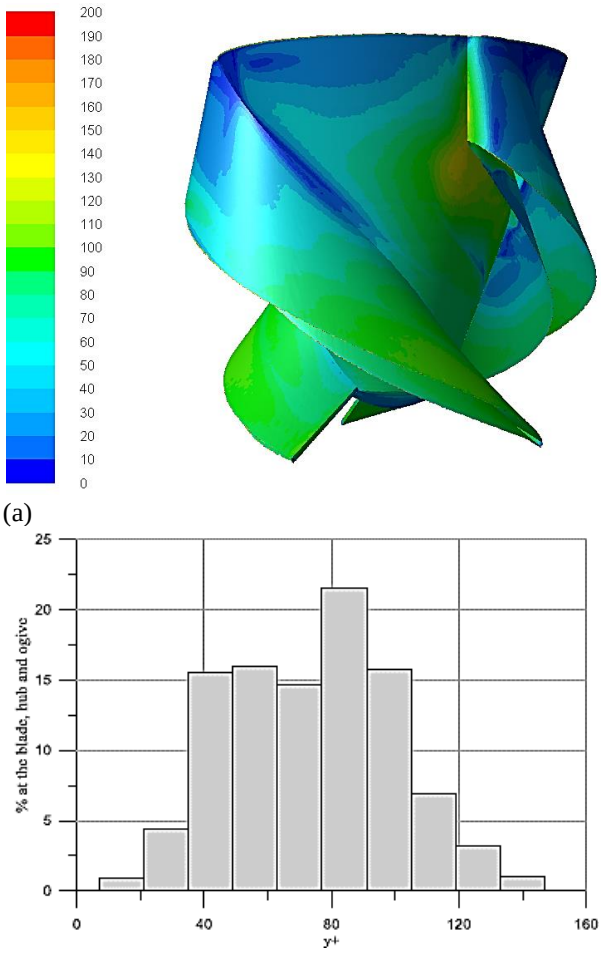

(a)

(b)

Fig. 17 (a) y^+ Distribution contours and, (b) y^+ values bar graph, for the Base Design of the Turbine Rotor Geometry

5. RESULTS

5.1 Characteristic Curves of the Base Design Turbine

The characteristic curves of the BD turbine, including hydraulic power, mechanical power, load, and hydraulic efficiency curves, are shown in Fig. (18). The hydraulic efficiency was calculated using Eq. (16), determined from the difference in total pressure between the turbine inlet and the draft tube outlet.

$$\eta_h = \frac{M\,\omega}{Q\Delta p_T} \tag{16}$$

The characteristic curves were obtained with continuity RMS residuals that reached $\in$=1x10^{-5}.

From Fig. 18, one can see that the volumetric flow design at 42.5 m³/s yielded a hydraulic efficiency of 76.64%, a shaft power of 34.54 MW, and a hydraulic power of 45.07 MW. These values are notably higher than those obtained for maximum efficiency, which was around 88.15%.

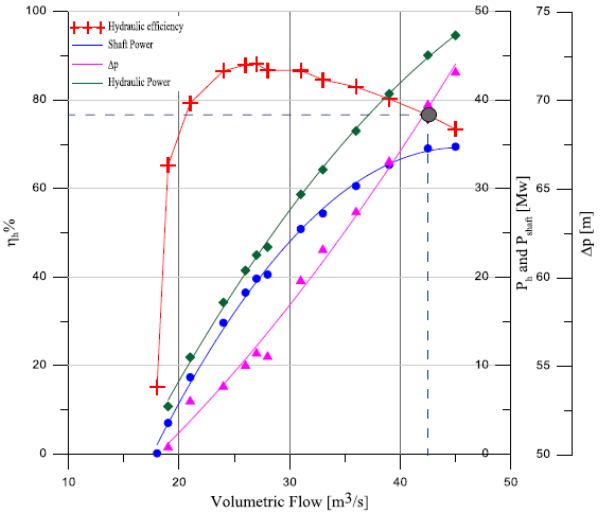

Fig. 18 Characteristic curves of the Performance of the BD turbine

Furthermore, the simulations for the BD turbine identified that the Best Efficiency Point (BEP) for a volumetric flow at Q = 27 m³/s was η_h = 88.15%, with shaft power at 19.83 MW and hydraulic power at 22.49 MW. Despite a significant difference between the flow design point and the flow for maximum hydraulic efficiency, with values ranging from 25 m³/s to 43 m³/s, this variation is explainable given that the shock effects at the turbine inlet were not considered in the preliminary design.

On the other hand, it was observed that the volumetric flow with the maximum hydraulic efficiency in the BD turbine is still within the operating range for this turbine type, as defined by Dixon and Dham (2011). The hydraulic efficiency result for this turbine is near the preliminary value at η_h = 90%, corroborating the findings of Hecker et al. (2005), who considered a fish-friendly turbine operating under Q = 28 m³/s, and a hydraulic head of 24 m. The results are also consistent with those obtained by Dixon and Dham (2011), with values for numerical hydraulic efficiency (CFD) at 94.05% (Q = 42.50 m³/s) and hydraulic efficiency at 93.10% in the test model.

These performance variations may be ascribed to differences in the rotor hydraulic channel design and the specific type of draft tube. For example, in Dixon and Dham (2011), a bifurcated draft tube was employed. Thus, in reference to the importance of the draft tube in the hydraulic performance of the turbine, a substantial influence was reported over the improvement in hydraulic efficiency. An increase in hydraulic efficiency of 5.49% was observed when comparing the original turbine draft tube initially used, with the final draft tube geometry in the numerical simulations, as reported by Dixon and Dham (2011).

The experimental validation of the turbine rotor's performance was outside the study scope in this study, given the substantial implementation costs and time required for test bench construction.

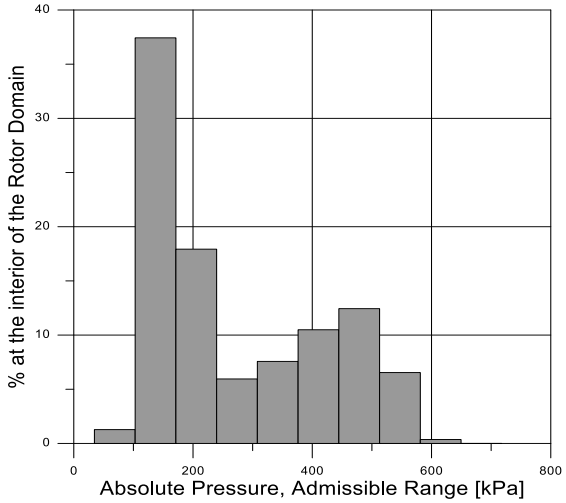

Fig. 19 Admissible range values for the Absolute Minimum Pressure

5.2. Assessment of the Fish-Friendly Turbine Parameter

The assessment of fish-friendly parameters, including absolute pressure, the rates of pressure variations, and the strain rate, was derived by post-processing the numerical simulations with the ANSYS Fluent® software program.

Minimum absolute Pressure.

The results for absolute pressure, considering standard atmospheric pressure at 1 atm, were obtained within the interior of the rotor domain, as shown in Fig. (19). The majority of these representative values fell within a range of 68.8 kPa to 752.02 kPa, corresponding to 100% in percentage terms that satisfy the Minimum Absolute Pressure Parameter, as referenced by Cooke et al. (2011) and Odeh (1999). These results are shown in Eq. (17) and align with findings from numerical simulations on the absolute pressure path lines through the rotor pass in the transitory regime, as shown by Hecker et al. (2012).

Pressure Variation Rate PVR and Strain Rate SR

To evaluate the other aforementioned parameters, like the pressure variation rate (PVR) and strain rate (SR), shown in Eq. (18) and Eq. (19) respectively, we determined the percentage of admissible values within the rotor domain. This was significant due to the importance of these phenomena within this domain. We then quantified the percentage of cells within the acceptable range for the strain rate and the pressure variation rate via post-processing in ANSYS Fluent®.

The pressure variation rate (PVR), using reference values cited in Hecker and Cook (2005), was established for salmon at a PVR limit value of 500 psi/s (3447.38 kPa/s), which significantly satisfies the fish survival criterion, as shown in Fig. (20). Regarding the strain rate, an acceptable value of 62.75% was found for the discretized rotor domain, satisfying requirements from Odeh (1999) and cited by Cooke et al. (2011), with an admissible value of 180 /s or less. A histogram of the

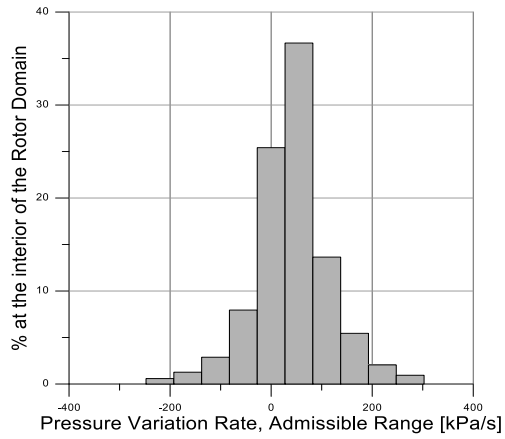

Fig. 20 Admissible range values for the Pressure Variation Rate.

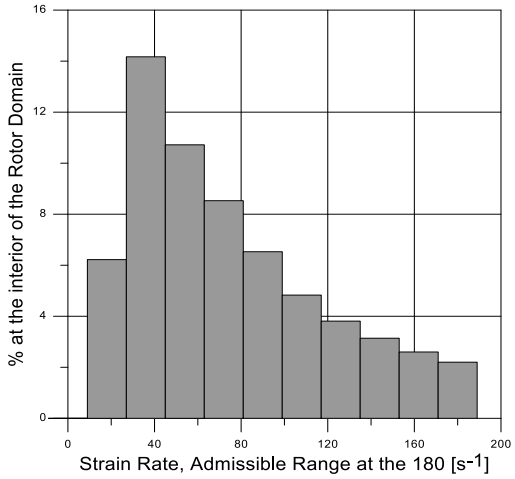

(a)

Fig. 21 a) Admissible range for the strain rate 180/s

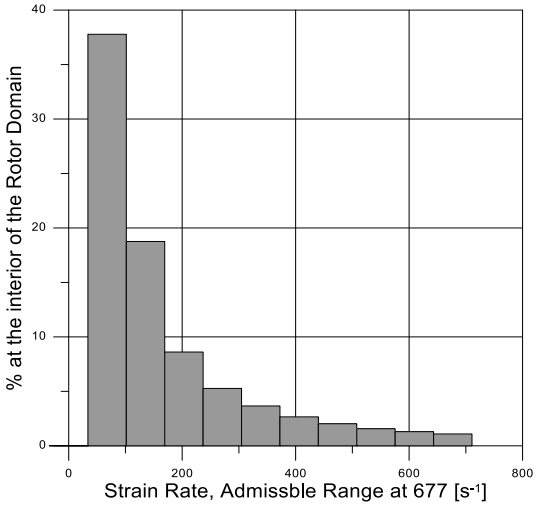

(b)

Fig. 21 b) Admissible range for the strain rate 677/s

strain rates up to 180 /s is given in Fig. 21a, with a reported value of 62.75% representing the total for 180 /s and greater. Other authors, considering different fish-friendly parameters, have suggested limits up to 600 /s, e.g., Deng et al. (2005). With a value of 677 /s, minimal injuries to the fish were observed without compromising chinook salmon survival, resulting in a satisfactory rate of 82.71%. This rate is likely to improve with enhanced hydraulic performance of the turbine rotor, as seen in Fig. 21b, which may further increase fish survival. An intermediate permissible strain rate of 360 /s to ensure fish survival was used by Dixon and Dham (2011).

Strain rates arising from shear stresses in the flow might be controlled by avoiding highly curvilinear flow or eddies, consistent with smooth flows through the turbine and efficient power conversions. Experimental studies involving fish introduced into water jets have demonstrated that there were no significant injuries to fish subjected to strain rates less than 500 /s, as reported by Neitzel et al. (2011).

5.3. Optimization Via DOE (Design of Experiments)

We should note that, before initiating the optimization process, certain geometric variables of the Preliminary Design Turbine (PD) were adjusted. This led us to create a new geometry, referred to as the Base Design turbine (BD), which was later integrated with Design of Experiments (DOE) as the optimization methodology.

The geometric variables subjected to the adjustment process included the variables $\beta_{4r\theta}$, $\beta_{5r\theta}$ (representing the relative flow angles), γ, δ (angles for constructing the hub geometry), and the geometric parameter c. The sweep angle, θ, and angle λ_4 values were fixed (the λ_4 value taken from the mid height of the blade), referencing the values from the fish-friendly Alden Voith turbine model, developed by Dixon and Dham (2011). The λ_5 angle was set at an initially determined value, and was subject to optimization via DOE in this subsection.

Design of Experiments (DOE) is an optimization technique that can be used to rapidly enhance a product or system's performance. As referenced by Uy and Telford (2009), DOE serves as a basis for conducting sensitivity studies or analyses on variables to comprehensively understand their impact on the performance of the product or system.

In this section, we will detail the optimization methodology based on DOE. Specifically, the selected geometrical design variables included the hydrofoil, the θ sweep angle and the λ_5 trailing edge angle of the blades. The control variables were defined as the fish survival parameters and hydraulic efficiency, with an emphasis on maximizing this function.

Hydrofoils: Hydrofoils with an approximately rounded leading-edge were taken to minimize the severity of injuries caused from fish impacts, as per Hecker et al. (2012). Consequently, three Göttingen hydrofoils were chosen. This methodology is adaptable and can be extended to other series like NACA, the CLARK family series, etc. The selected hydrofoils included the Göttingen 408, 474, and 622.

Sweep angle of the blade θ: the variation limits for θ were established from 171° to 200°, with intermediate values at 180°, 189°, and 195°. Angle θ directly influences

Table 9 Design variables

Goe	408		474	622	
θ^{o}	171	180	189	195	200
λ_5^{o}	53	58	63	68	72

either an increase or decrease in friction, since it is related to the length of the rotor hydraulic channel.

Trailing edge angle of the blade, λ_5: the trailing edge angle of the blade varied from λ_5=53º to λ_5=72º, with intermediate values at 58°, 63°, and 68°. This angle directly affects the rotor height and implicitly defines the progressive increase of torsion along the channel's entire length, which may influence the hydraulic performance. Table 9 summarizes the design variables information.

The set of design variables was chosen considering the most critical variables for either improving or worsening hydraulic efficiency, along with any influence on the hydraulic channel. Consequently, a three-variable factorial DOE was constructed, encompassing the hydrofoil, the sweep angle θ, and the trailing edge angle λ_5 of the blades, resulting in 67 geometries.

5.4. Evaluation of the Fish Survival Parameters in the Fish-Friendly Turbine

Another optimization process procedure employed here was the Weighted Sum Method optimization technique. This method is used for Multi-Objective Optimization Problems with lateral constraints, as mentioned in Deb (2001), and is suitable for optimizing hydraulic efficiency and fish-friendly parameters in turbines, with lateral constraints in the optimization process. This method was applied to the DOE outcomes in this study. Along with hydraulic efficiency, optimal performance must also include fish-friendly parameters like minimum absolute pressure, strain rate (SR), and pressure variation rates (PVR) in the turbine's design, as expressed in Eq. (17) through Eq. (19).

$$P_{Min\,abs.} \geq 68{,}8\ kPa \tag{17}$$

Where the $P_{Min\,Abs.}$ is the minimum absolute pressure,

$$PVR \rightarrow w\frac{dp}{ds} = \left(\left(w_x \frac{dp}{dx} \right)^2 + \left(w_y \frac{dp}{dy} \right)^2 + \left(w_z \frac{dp}{dz} \right)^2 \right)^{1/2} \leq 550.3\ kPa/s \tag{18}$$

Where $w\frac{dp}{ds}$ is the pressure variation rate (PVR)

$$SR \rightarrow \varepsilon = \frac{dV}{dS} \leq 180\ s^{-1} \tag{19}$$

Where ε is the strain rate (SR).

Due to the lateral constraints of the admissible values for fish survival rates (see Eq. (17) through Eq. (19)), we needed to quantify the percentages of these variations within the rotor domain. Therefore, reference indicators for the minimum absolute pressure, the pressure variation rate, and the strain rate were created. These indicators were derived from post-processing in ANSYS Fluent® using the Main Field Function tool, as shown in (Fig. 19), which gives a histogram of the absolute pressure values within the admissible range, where the sum of all the compartments equals 100%. However, we should note that the minimum admissible value for a given variable may lead to percentage values equal to or less than 100% for the indicators in each geometry. The following indicators can, therefore, be defined:

- Ind $_{\text{Abs. Min. P.}}$ = Minimum Absolute Admissible Pressure Indicator at the rotor domain (%);
- Ind $_{\text{ST}}$ = Admissible Strain Rate Indicator at the rotor domain (%); and
- Ind $_{\text{PVR}}$ = Admissible Pressure Variation Rate Indicator at the rotor domain (%).

Additionally, pondered weights were imposed for each of the output variables of interest (hydraulic efficiency, strain rate, and pressure variation rate) during the optimization process through a DOE. Given the outcomes of the DOE, all geometries concerning the Minimum Absolute Admissible Pressure Indicator reached 100%; therefore, we did not need to include the pondered weight procedure for this variable, since the geometries entirely satisfied the absolute minimum pressure requirement.

The output variables were, therefore, defined as hydraulic efficiency, with weight w_{nh} = 0.64; the Admissible Strain Rate Indicator, with weight w_{ST} = 0.27; and the Admissible Pressure Variation Rate Indicator, with weight w_{PVR} = 0.09. We should also note that the greatest weight was attributed to hydraulic efficiency, given its significance in terms of energy generation. The other weights for the Admissible Strain Rate and Admissible Pressure Variation Rate Indicators were determined and assigned based on the substantially different orders of magnitude at which they were satisfied. Thus, the highest value of the weighted average that defined the optimized geometry of the fish-friendly turbine was as follows:

$$Weight\ Sum\ Indicator = w_{nh}\eta_h + w_{ST}\,Ind_{ST} + w_{PVR}\,Ind_{PVR} \tag{20}$$

It is very important to emphasize that we selected these weights based on the specific criteria in our present study. Other researchers might estimate different weight values according to their preferences and particular studies.

5.5. Optimized Geometry Turbine Via DOE

Using the weight sum procedure on the DOE, geometries were identified that reached the highest values for the weight sums, using the previously established weights (Table 10). The fish-friendly turbine geometry that showed a maximum value for the weighted WSI sum was the turbine with Göttingen 622 hydrofoils, a sweep angle at θ=180°, and a trailing edge angle at λ_5=53°.

DOE geometries with the Goe 622 and Goe 474 hydrofoils, were obtained with Continuity RMS residuals that reached $\in$=1x10-5. For the Goe 408 hydrofoil, the convergence residuals were below $\in$=2x10-5.

Table 10 DOE Designs with the highest admissible averaged weight values

Rotor Geometry	η_h %	Strain Rate Indicator%	Pressure Variation Rate Indicator %	Averaged Weight Eq. (21)
Goe 622: λ_5=53°: θ=180°	88.26	62.63	97.00	82.13
Goe 622: λ_5=58°: θ=180°	88.15	62.75	96.86	82.08
Goe 622: λ_5=53°: θ=200°	88.74	60.06	96,65	81,71

Table 11 Geometrical Design Variables for the OG turbine rotor

Blade Width, [m]	Hub Angles [°]	Angle θ [°]	Angles $\beta_{r\theta}$ [°]	Goe	Angles λ [°]	N_{Blade}	$D_{medium\ point}$
b_4=1.012 b_5=1.190	δ=70 γ=89	180	$\beta_{4r\theta}$=19 $\beta_{5r\theta}$=20	622	λ_4=4,5 λ_5=53	3	0.7D_{AB}

Table 12 Basic Dimensions of the OG turbine rotor

D_{4i} [m]	D_{4m} [m]	D_{4e} [m]	D_{5i} [m]	D_{5m} [m]	D_{5e} [m]	h_{hub} [m]
3.7480	3.8274	3.9069	1.1618	2.1707	3.1795	3.713

Table 13 Determining the suction height in the OG turbine rotor

b_{4h} [m]	h_{Dr} [m]	h_{Drn} [m]	$h_{Draft\ tube}$ [m]	h_{water} [m]	p_7 [Pa]
1.009	5.241	4.737	6.33	11.067	103.406,81

For OG turbine are listed in the Table 11 and Table 12, the geometrical design variables and basic dimensions for the rotor, respectively, as well its suction head, see Table 13.

5.6. Analysis of the Main Effects and Interactions of the Variables Involved in the DOE

Based on the DOE, which consisted of 67 experiments, it is feasible to present an analysis of the main effects and the interactions between the variables involved. The MINITAB® software program was used to study the primary effects of the parameters (hydrofoil, sweep angle, θ, and trailing edge angle, λ_5) and the interactions among them. In the analysis of the main effects, the averages of each output variable—namely, hydraulic efficiency, and the fish survival indicator parameters relative to the input variables—were determined (see Fig. 22 a-c).

An analysis of the influence of the input variables and their interactions on each of the output variables was conducted using the Standardized Effects Pareto (Fig. 23a, through Fig. 23d), represented using bar charts.

Standardized effects are defined as the values acquired for each normalized input variable, divided by the respective standard deviations for each variable, within a defined confidence interval, i.e., the t-student probabilistic distribution. A 95% confidence interval was chosen. This statistical analysis was performed on the output variables of greatest relevance in the performance behavior, in accordance with the results obtained from the DOE.

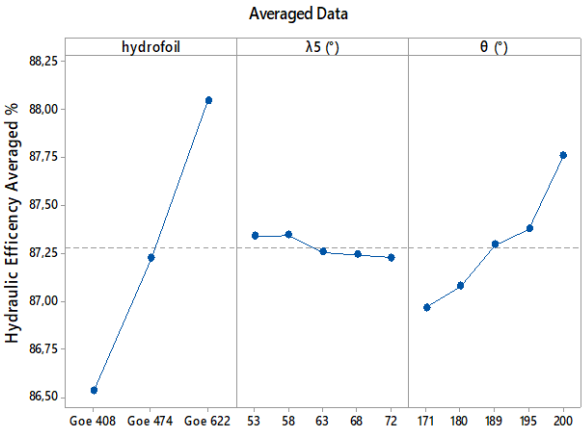

Fig. 22 a) Main Effects on Hydraulic Efficiency

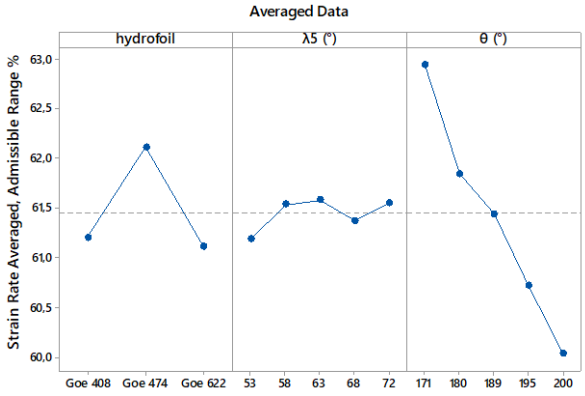

Fig. 22 b) Main Effects on the Admissible SR Indicator

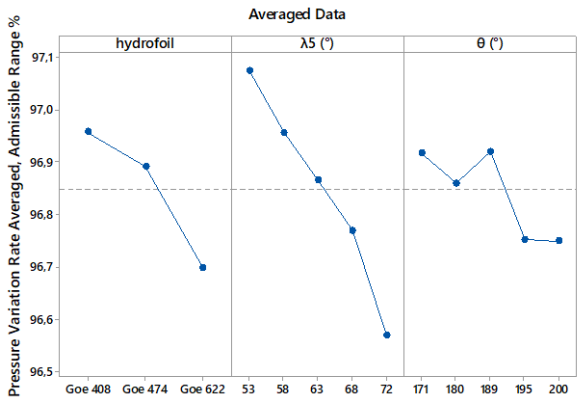

Fig. 22 c) Main Effects on the Admissible PVR Indicator

With regard to the main effects on the Hydraulic Efficiency values, there was a consistent trend towards an increasing value, depending on the hydrofoil type and the increment in the sweep angle θ (see Fig. 22a).

Conversely, for the effects on the Admissible Strain Rate indicator (SR), variations appeared to depend primarily on the sweep angle θ and hydrofoil type. Regarding the influence of angle λ_5 on the Admissible Strain Rate indicator (SR), no defined tendency was observed (Fig. 22b).

Regarding the main effects of the Pressure Variation Rate (PVR), and upon analyzing the results shown in Figs 22a and 22c, one can see that the admissible PVR Indicator decreased the more hydraulically efficient the hydrofoil. Regarding the trailing edge angle λ_5 and the sweep angle θ of the blades, the Admissible PVR Indicator decreased when angles λ_5 and θ increased, resulting in a slight way, less friendly for the fish survival (Fig. 22c) and angle λ_5, as well as interactions between angle λ_5 and the sweep angle θ of the blades, was less significant (Fig. 23a).

The hydrofoil type can either positively or negatively affect hydraulic efficiency, due to variations in the leading edges that can generate regions of boundary layer separation. Conversely, increasing the sweep angle will enhance hydraulic efficiency, since it increased the moment transferred from the flow to the turbine rotor. With respect to angle λ_5, hydraulic efficiency increased as this angle decreased (See Fig. 10).

Regarding the behavior of the allowable SR indicator, the most influential factor initially was the blade sweep angle θ, followed by the hydrofoil type. Interactions between other geometric variables can be considered inconsequential, as shown in Fig. 23b. With an increase in the sweep angle, the channel length grew, leading to an increase in shear stress rates.

Regarding the Admissible PVR Indicator, the primary directly influencing factor was the trailing edge angle of the blade λ_5, followed by the hydrofoil type and sweep angle. Additionally, the interaction between the hydrofoil type and the trailing edge angle λ_5 stood out, since it increased the admissible PVR Indicator values

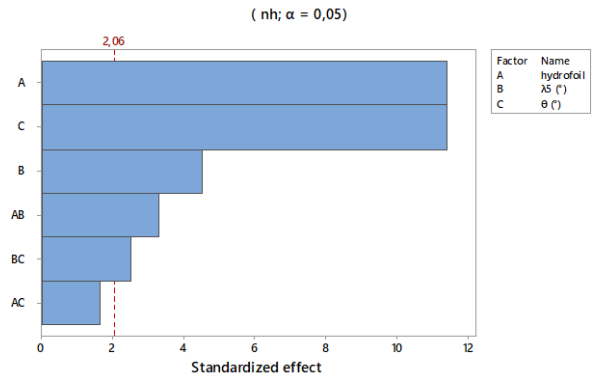

Fig. 23 a) Standardized effect Pareto charts for Hydraulic Efficiency

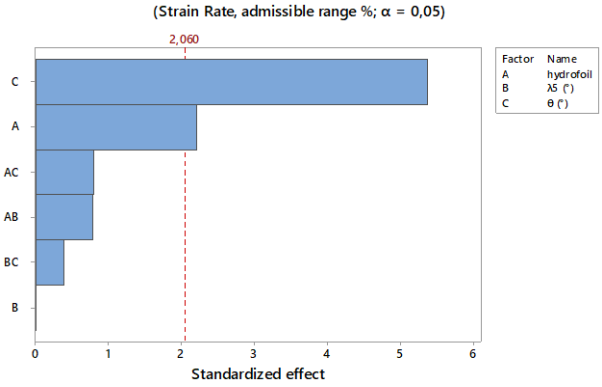

Fig. 23 b) Standardized effect Pareto charts for the Admissible SR Indicator

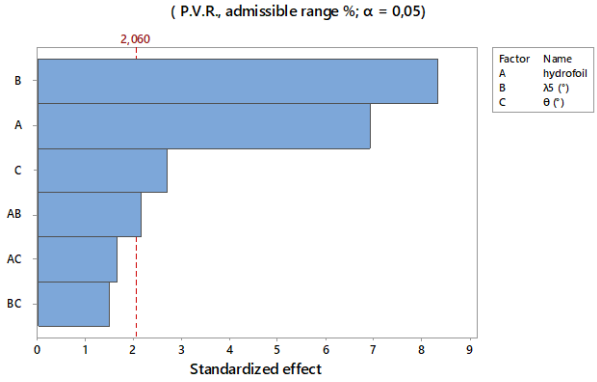

Fig. 23 c) Standardized effect Pareto charts for the Admissible PVR Indicator

when is used a less efficient hydrofoil and the magnitude of λ_5 decreases, and vice versa.

Based on Figs 23a-c, one may draw certain conclusions. The most pronounced geometric effect on the three indicators, in general, was imparted by the sweep angle, followed by the hydrofoil type, and to a lesser degree, by the trailing edge angle, respectively.

5.7. Hydraulic Efficiency Curve for the Optimized Geometry Turbine.

The characteristic curves for hydraulic efficiency as a function of the volumetric flow of the rotor were obtained for the Preliminary Design Turbine (PD), Base

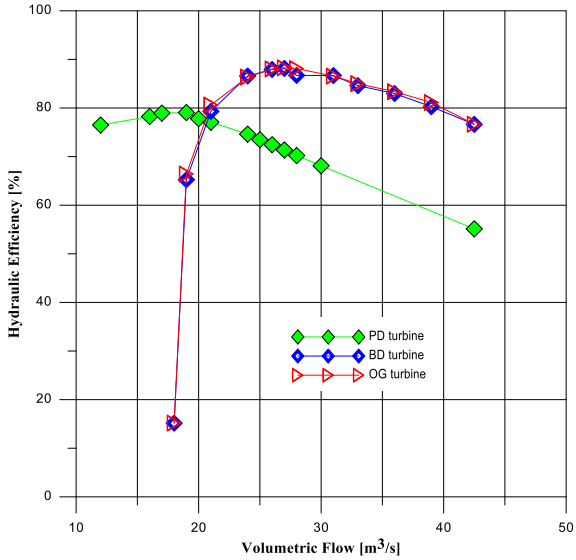

Fig. 24 Comparison of Hydraulic Efficiency Vs Volumetric Flow between the turbine geometries

Table 14 Performance outcomes of the turbines for the Project Design Point, and Volumetric Flow *Q*=42.5m3/s

Geometry	Hydraulic Power [MW]	Shaft Power [MW]	Hydraulic Efficiency [%]
PD turbine	11.65	6.42	55.14
DB Turbine	45.07	34.54	76.64
OG Turbine	45.73	35.06	76.67

Table 15 Performance outcomes of the turbines for the BEP

Geometry	Hydraulic Power [MW]	Shaft Power [MW]	Hydraulic Efficiency [%]	Q at the BEP [m³/s]
PD turbine	5.21	4.12	79.06	19
DB Turbine	22.49	19.83	88.15	27
OG Turbine	22.82	20.14	88.26	27

Design Turbine (BD), and the Optimized Geometry Turbine (OG) (Fig. 24).

Simultaneously, the results from the PD, BD, and OG turbines were reported at the design point operation for the volumetric flow Q=42.5m³/s, as well as for the BEP in each turbine geometry, encompassing Hydraulic Power, Shaft Power, and Hydraulic Efficiency. See Table 14 and Table 15.

Regarding the PD turbine, the results for hydraulic performance at the design point Q=42.5 m³/s indicated Hydraulic Efficiency at 55.14%, with hydraulic power at 11.65 MW and Shaft Power at 6.42 MW. However, the highest Hydraulic Efficiency (79.06%) occurred for a volumetric flow at 19 m³/s, resulting in shaft power values at 4.12 MW and Hydraulic Power at 5.21 MW. See Table 14 and Table 15.

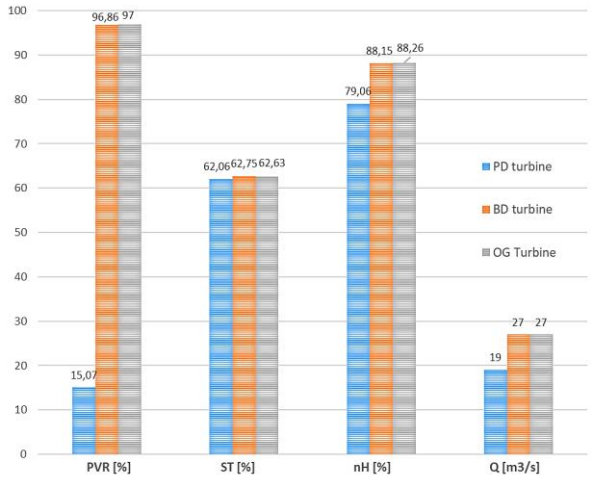

Fig. 25 Comparative bar charts from the optimization processes of the fish-friendly turbine

Convergence for the PD turbine at the mass criterion was achieved with continuity RMS residuals that reached $\in$=2x10^{-5} for the BEP, and at the design point Q=42.5 m³/s with continuity RMS residuals that reached $\in$=1x10^{-4}, respectively. For other points of the Hydraulic Efficiency versus Volumetric flow for the PD turbine, convergence at the mass criterion was reached with continuity RMS residuals below $\in$=5x10^{-5}.

Regarding the results of the numerical simulations on the characteristic curves of the BD Turbine at the design point Q=42.5 m³/s, hydraulic efficiency at 76.64% was achieved, along with hydraulic power at 45.07 MW and shaft power at 34.54 MW.

The BD Turbine, with a volumetric flow at Q=27 m³/s, reached maximum hydraulic efficiency at 88.15%, with hydraulic power at 22.49 MW, and shaft power at 19.83 MW (see Fig. 18).

For the OG Turbine, the numerical simulations showed a slight improvement in hydraulic efficiency above the BD Turbine. At design point Q=42.5 m³/s, hydraulic efficiency was 76.67%, hydraulic power was 45.73 MW, and shaft power was 35.06 MW. Similarly, at the point of maximum efficiency for volumetric flow Q=27 m³/s, hydraulic efficiency was 88.26%, hydraulic power was 22.82 MW, and shaft power was 20.14 MW (see Fig. 24).

Considering the shaft power at the BEP for the analyzed turbine geometries, a shaft power gain of 13.41 MW was observed between the PD Turbine and the BD Turbine, respectively. Meanwhile, there was a shaft power gain of 0.31 MW between the BD Turbine and the OG Turbine, respectively. The shaft power gain between the PD Turbine and the OG Turbine was 13.72 MW.

In Fig. 25, the results showed a significant improvement was through all optimization processes applied to the PD turbine and to the OG turbine, in the PVR admissible indicator from 15.07% to 97% within the Rotor Domain. Concurrently, there was a substantial improvement in Hydraulic Efficiency from 79.06% to 88.26%, along with an increment in Volumetric Flow at

the BEP of the turbine rotor, from Q=19 m³/s to Q=27 m³/s, from the PD turbine to the OG turbine.

In recognizing the nature of Multi-Objective Optimization processes, contradictory goals could be present in optimization processes. This was the case with the ST admissible Indicator; although a slight improvement was observed from the PD Turbine to the BD Turbine, a minor decrease occurred between the BD Turbine and the OG turbine, with the former being slightly more efficient than the OG Turbine (see Fig. 25).

Evidently, a significant difference exists between the volumetric flow of design and the volumetric flow at the BEP (Best Efficiency Point) for all turbine geometries, with a larger discrepancy between the PD Turbine and both other turbine geometries (BD turbine and OG turbine). However, as shown in Fig. 24 and Fig. 25, the maximum efficiencies were maintained between 25 m³/s and 43 m³/s for the DB and OG turbines, respectively. As was previously noted, this variation (in both the BD turbine and the OG turbine) may be attributed to the fact that the design does not account for flow shocks. Since the Fish Friendly Turbine has only three blades, these geometries are more sensitive to shock conditions. Consequently, the flow incidence on the rotor was more significant for both the meridional velocity and the volumetric flow, respectively.

Although differences exist between the design point operation and maximum efficiency in volumetric flow across all turbine geometries (PD turbine, BD turbine, and the OG turbine), operation remained within the practical limits for these turbines, as was also shown by Dixon and Dham (2011) (see Fig. 1).

Based on the results from Dixon and Dham (2011), maximum hydraulic efficiency at 94.05% was reached in the numerical simulations for Q=42.5 m³/s for the prototype, and hydraulic efficiency at 93.10% was achieved with a reduced model tested. Considering the two turbines (the Alden Voith turbine and the OG turbine), there was a difference of 5.79%. This discrepancy might be attributed to variations in the rotor hydraulic channel design and the type of draft tube with its outlet divided by a longitudinal septum in the Alden Voith Turbine, as developed by Dixon and Dham (2011).

5.8. Flow Field Analysis for the Optimized Geometry Turbine

Regarding the flow field analysis for the OG turbine rotor, the contours of the total pressure are shown in Fig. 25. One can see that the stagnation pressure was focused at the leading edges of the blades, which is desirable for a turbine rotor at its BEP (Best Efficiency Point), without shocks.

Figure 26 shows the flow velocity variations through the OG turbine rotor and a decrease in the flow velocity magnitude along the rotor height. A semi-axial outflow was observed, with higher velocity magnitudes at the trailing edges, at the tips of the blades. Concurrently, a vortex was observed at the rotor ogive that extended downstream from the rotor, creating a low-velocity region along the propagation path.

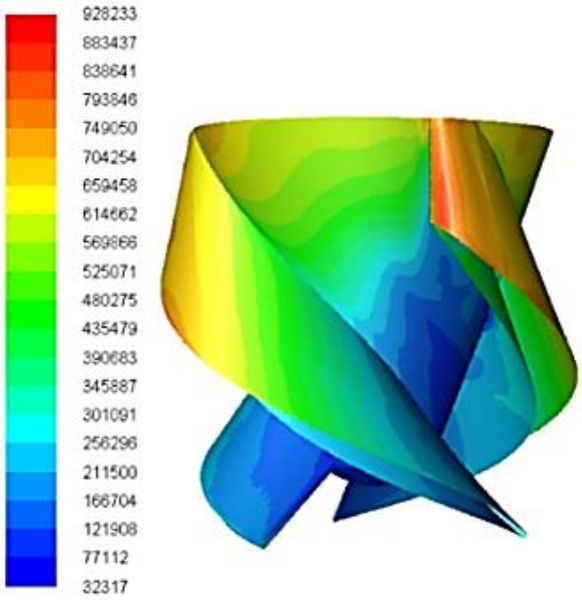

Fig. 26. Contours of the Total Pressure for the OG turbine rotor via DOE [Pa].

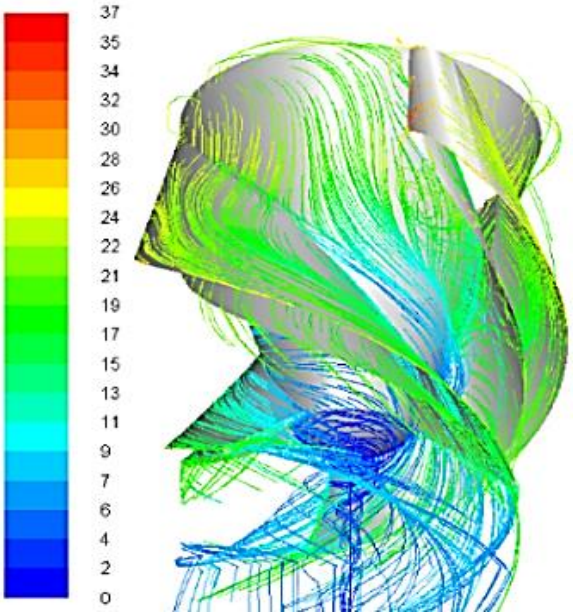

Fig. 27. Velocity path lines for the OG turbine rotor via DOE [m/s].

In Figs 26 and 27, showing the OG turbine rotor, the greatest magnitude velocity lines are shown to be generated close to the leading edges of the blades, i.e., the region corresponding to stagnation pressure. This phenomenon can be attributed to a small zone of flow acceleration in these areas, in function of the presence of an adverse pressure gradient.

6. CONCLUSIONS

This study introduced a methodology for a fish-friendly turbine rotor design, based on the geometric parametrization of both hub and blade generation. This approach resulted in substantial improvements to hydraulic performance, power generation, and fish-

friendly features, from the initial version (the Preliminary Design Turbine Geometry) to the Optimized Turbine Geometry.

Furthermore, we emphasized the importance of the geometric variables involved in the hub and blade generation when designing fish-friendly turbine rotors. These variables significantly influence highly efficient turbine rotor geometries, reaching both high-power generation and maintaining high fish survival rates, all within fish-friendly standards.

Regarding the variables selected for the DOE, the type of hydrofoils, the sweep angle θ, and angle λ_5 were found to affect the hydraulic performance of the turbine and the fish-friendly behavior of the turbine rotor. These can be used to design turbine rotors with high hydraulic performance while simultaneously improving fish survival rates during rotor passage.

While a turbine rotor with acceptable hydraulic performance has been identified for the design operating point of the turbine, we advise engaging in optimization studies. This process could extend beyond the results obtained from the sensitivity analysis of the hub construction angles and the geometric parameter *c*. In the current methodology, these geometric parameters impacted the volumetric flow rate passing through the runner, thus influencing both hydraulic performance and energy production.

For subsequent studies, we recommend considering the significance of the draft tube geometry on the hydraulic performance of this type of fish-friendly turbine. One possible line of research on this subject could include developing projects related to applying the current fish-friendly turbine rotor design methodology, complemented by creating a draft tube geometry that enhances the hydraulic performance of the turbine.

ACKNOWLEDGMENTS

Thanks to CAPES and FAPEMIG for financially supporting this study. This study was developed in the LHV (Virtual Hydrodynamic Laboratory) at UNIFEI (Federal University of Itajubá), Brazil.

CONFLICT OF INTEREST

The authors declare that they have no competing interests.

AUTHORS CONTRIBUTION

G. E. Niño Del Río: Conceptualization, Methodology, Investigation, Formal analysis, Validation, Writing - original draft, Writing-review & editing. **R. G. Ramírez Camacho**: Conceptualization, Supervision, Resources, Methodology, Writing - original draft. **N. Manzanares Filho**: Conceptualization, Supervision, Methodology. W. de Oliveira: Methodology, Conceptualization. **T. M. Arispe Angulo**: Methodology, Writing-review & editing.

REFERENCES

Abernethy, C., Amidan, B., & Čada, G. (2003). *Fish passage through a simulated horizontal bulb turbine pressure regime: a supplement to laboratory studies of the effects of pressure and dissolved gas supersaturation on turbine-passed fish*. Pacific Northwest National Laboratory. https://doi.10.2172/15004163.

Abernethy, C., Amidan, B., & Čada, G. (2002). *Simulated passage through a modified kaplan turbine pressure regime: a supplement to laboratory studies of the effects of pressure and dissolved gas supersaturation on turbine-passed fish***.** Oak Ridge National Laboratory and Pacific Northwest National Laboratory Richland, Washington. https://doi.10.2172/15001623.

Aguirre, C. A., Ramirez Camacho, R. G., De Oliveira, W., & Abellan, F. (2019). Numerical analysis for detecting head losses in trifurcations of high head in hydropower plants. *Renewable Energy*, *131*, 197-207. https://doi.org/10.1016/j.renene.2018.07.021.

Amaral, S., Hecker, G., & Pioppi, N. (2011). *Fish passage through turbines: Application of conventional hydropower data to hydrokinetic technologies*. Final Report No. 1024638, Alden Research Laboratory.

Arispe, T. M. (2016). *Obtainment of performance characteristic of francis turbine and draft tube parameterization using computational fluid dynamic techniques*. [MSc. Dissertation, Instituto de Engenharia Mecânica, Universidade Federal de Itajubá]**.** Itajubá, Minas Gerais, Brazil.

Arispe, T. M., Oliveira, W., & Ramirez Camacho, R. (2018). Francis turbine draft tube parameterization and analysis of performance characteristics using CFD techniques. *Renewable Energy*, *127*, P.114-124. https://doi.org/10.1016/j.renene.2018.04.055

Bardina, J., Huang, P. G., Coakley, T. (1997). Turbulence modeling validation, testing and development. *NASA Technical memorandum*, 110446.

Becker, C. S., Abernethy, J. M., & Dauble, D. D. (2003). Identifying the effects on fish of changes in water pressure during turbine passage. *Hydro Review*, *22* (5), 32-42.

Bran, R., & De Sousa, Z. (1969). *Máquinas de Fluxo Turbinas-Bombas-Ventiladores*. Editorial Ao livro Técnico S. A., Rio de Janeiro.

Brown, R., Colotelo, A., Pflugrath, B., Boys, C., Baumgartner, L., Deng, D., Silva, L., Brauner, C., Mallen-Cooper, M., Phonekhampeng, O., Thorncraft, G., & Singhanouvong, D. (2014). Understanding barotrauma in fish passing hydro structures: A global strategy for sustainable development of water resources, *Fisheries*, *39*(3), 108-122. https://doi.org/10.1080/03632415.2014.883570

Brown, R., Pflugrath, B., Colotelo, A., Brauner, C., Carlson, T., Deng, Z., & Seaburg, A. (2012). Pathways of barotrauma in juvenile salmonids exposed to simulated hydroturbine passage: Boyle's law vs. Henry's law. *Fisheries Research*, *121-122*, 43–50. https://doi.org/10.1016/j.fishres.2012.01.006

Čada, G. (2001). The development of advanced hydroelectric turbines to improve fish passage survival. *Fisheries*, *26*(9). https://doi.org/10.1577/1548-8446(2001)026<0014:TDOAHT>2.0.CO;2

Cook, T., Cain, S., Fetfatsidis, P., Hecker, G., & Stacy, P. **(**2000). *Final turbine and test facility design report Alden/NREC fish friendly turbine*. Alden Research Laboratory, Inc. Northern Research and Engineering Corporation. https://doi.org/10.2172/1218145

Cooke, S., Hatry, C., Hasler, C., & Smokorowski, K. (2011). Literature review, synthesis and proposed guidelines related to the biological evaluation of "fish friendly" very low head turbine technology in Canada. *Canadian Technical Report of Fisheries and Aquatic Sciences*, 2931.

Deb, K. (2001). *Multi-objective optimization with evolutionary algorithms*. John Wiley and Sons Ltda.

Deng, Z., Guensch, G., Mc Kinstry, C., Mueller, R., Dauble, D., & Richmond, G. (2005). Evaluation of fish-injury mechanisms during exposure to turbulent shear flow. Canadian Journal of Fisheries and Aquatic Sciences *62*(7). https://doi.org/10.1139/f05-091

Dixon, D., & Dham, R. (2011). *Fish friendly hydropower turbine development and deployment alden turbine preliminary engineering and model testing*. Electric Power Research Institute and US. Department of Energy. Electric Power Research Institute, California. USA. https://doi.org/10.2172/1050066

Fu, T., Deng, Z., Duncan, J., Zhou, D., Carlson, T., Johnson, G., & Hou, H. (2016). Assessing hydraulic conditions through Francis turbines using an autonomous sensor device. *Renewable Energy*, *99*, 1244 -1252. https://doi.org/10.1016/j.renene.2016.08.029

Hecker, G., & Cook, T. (2005). Development and evaluation of a new helical fish friendly hydroturbine. *Journal of Hydraulic Engineering ASCE*, *131*(10), 835-844. https://doi.org/10.1061/(ASCE)0733-9429(2005)131:10(835)

Hecker, G., Amaral, S., Allen, G., Li, S., Perkins, N., & Dixon, D. (2012). *The science behind a fish friendly turbine. National Conference on Engineering and Ecohydrology for Fish Passage*, U. Mass Amherst.

Hou, H. C., Zhang, Y. X., Xu, C., Zhang, J. Y., & Li, Z. L. (2016). *Effects of radial diffuser hydraulic design on a double suction centrifugal pump*. IOP Conf. Series: Materials Science and Engineering. https://doi.10.1088/1757-899X/129/1/012017

Hydro Power Plant Oeblitz (2017). *Europe's most fish-friendly hydro power plant*. DIVE Turbinen GmbH & Co. KG. Audiovisual media.

Langford, M. T., Zhu, D. Z., & Leake, A. (2015). Upstream hydraulics of a run-of-the river hydropower facility for fish entrainment risk assessment. *Journal of Hydraulic Engineering ASCE*. *142* (4), 05015006. https://doi.org/10.1061/(ASCE)HY.1943-7900.0001101

Larinier, M., & Dartiguelongue, J. (1989). The Circulation of Migratory Fish: Transit through the turbines of Hydroelectric Installations. *Bull. FT. Pêche Piscic.* 312 - *313*, 1-87. https://doi.org/10.1051/kmae:1989011

LEAP CFD TEAM (2012). *Tips & Tricks: Convergence and Mesh Independence Study.*

Loures, R. (2012). Desenvolvimento de metodologia para avaliação de riscos de impactos diretos de Usinas Hidrelétricas sobre a ictiofauna. III Seminário Estratégias para Conservação de peixes em Minas Gerais.

Ludewig, P., Hecker, G., Perkins, N., & Jacobson, P. (2018). Considering the Alden Turbine for a Plant Rehab. Hydro Review. *North America, Rehabilitation and Repair, Turbines and Mechanical Components*, *3*(37).

Macintyre, A. (1987). *Máquinas Motrizes Hidráulicas.* Editorial Guanabara Dois S.A. Rio de Janeiro.

Menter, F., Kuntz, M., & Langtry, R. (2003). Ten years of experience with the SST Turbulence model**.** *Turbulence, Heat and Mass Transfer*, *4*(1), 625-632.

Mueller, M., Pander, J., & Geist, J. (2017). Evaluation of external fish injury caused by hydropower plants based on a novel field-based protocol. *Wiley Fisheries Management and Ecology Journal*, 24, 240–255. https://doi.org/10.1111/fme.12229

Neitzel, D., Dauble, D., Čada, G., Richmond, M., Guensch, G., Mueller, R., Abernethy, C., & Amidan, B. (2011). Survival estimates for juvenile fish subjected to a laboratory-generated shear environment. *Transactions of the American Fisheries Society*, *133*(2), 447-454. https://doi.org/10.1577/02-021

Nielsen, N., Brown, R., & Deng, D. (2015). Review of existing knowledge on the effectiveness and economics of fish-friendly turbines. Technical Paper, *Phnom Penh, Mekong River Commission* 57.

Niño Del Río, G. E. (2018). Project methodology of a fish friendly turbine through optimization technics based in design of experiments. [DSc. Thesis, Instituto de Engenharia Mecânica, Universidade Federal de Itajubá]. Itajubá, Minas Gerais, Brazil.

Nuernbergk, D., & Rorres, C. (2013). Analytical model for water inflow of an archimedes screw used in hydropower generation. *Journal of Hydraulic Engineering ASCE*. *139*(2), 213-220.

https://doi.org/10.1061/(ASCE)HY.1943-7900.0000661

Odeh, M. (1999). *Hydropower a summary of environmentally friendly turbine design concepts*. Developed by Alden Research Laboratory, Inc., Voith Hydro, Inc. and their Teams for United States Department of Energy Idaho Operations Office. https://doi.org/10.2172/1218115

Ploskey, G., & Carlson, T. (2004). *Comparison of Blade-Strike Modeling Results with Empirical Data*. Pacific Nothwest National Laboratory.

Richmond, M., Serkowski, J. A., Ebner, L. L., Sickc, M., Brown, R. S., & Carlson, T. J. (2014). Quantifying barotrauma risk to juvenile fish during hydro-turbine passage. *Fisheries Research journal*, *154*, 152–164. https://doi.org/10.1016/j.fishres.2014.01.007

Schmalz, W. (2010). Investigations into fish descent and control of possible fish damage caused by the hydropower screw at the Walkmühle hydroelectric power plant on the Werra in Meiningen—fish ecology and limnological research center in southern Thuringia. Thuringian State Institute for Environment and Geology, Jena.

Silva, E. R., Manzanares Filho, N., & Ramirez, R. (2012). Metamodeling approach using radial basis functions, stochastic search algorithm and CFD application to blade cascade design. *International Journal of Mathematical Modelling and Numerical Optimization.* https://doi.org/10.1504/IJMMNO.2012.044715

Srinivasan, K. M. (2008). *Rotodynamics pumps (Centrifugal and Axial)*. Mechanical Sciences Department of Mechanical Engineering. Kumaraguru College of Technology, Coimbatore, Tamil Nadu. New Age International (P) Ltd., Publishers.

Trumbo, B., Ahmann, M., Renholds, J., Brown, R., Colotelo, A., & Deng, Z. (2014). Improving hydroturbine pressures to enhance salmon passage survival and recovery. *Reviews in Fish Biol Fisheries Journal*, *24*, 955–965. https://doi.org/10.1007/s11160-013-9340-8

U.S. Corps of Army Engineers (2016). New Turbines Improves Fish Passage. – WALLA WALLA DISTRICT 201 North Third Avenue; Walla Walla, WA 99362.

Uy, M., & Telford, J. K. (2009) *Optimization by design of experiment techniques*. IEEE Aerospace Conference, Big Sky, MT, USA. https://doi.10.1109/AERO.2009.4839625

Vivier, L. (1966). *Turbines hydrauliques et leur régulation*. Albin Michel, Paris.

Watson, M. (1995). *Allowable Gas Supersaturation for Fish Passing Hydroelectric Dams. Project No. 93-8. Final Report Prepared For Bonneville Power Administration, U.S. Department Of Energy, Portland, Oregon.*